Design of a Fully Compliant Under-Actuated Finger with a Monolithic Structure and Distributed Compliance

Peter Steutel

Delft University of Technology 2010

Design of a Fully Compliant Under-Actuated Finger with a Monolithic Structure and Distributed Compliance

Master thesis Biomechanical Engineering

Exam committee:

Prof.dr. F.C.T. van der Helm, Biomechanical Engineering, TU Delft
Dr.ir. J.L. Herder, Biomechanical Engineering, TU Delft
Ir. G.A. Kragten, Biomechanical Engineering, TU Delft
Dr.Ir. J.F.L. Goosen, Fundamentals of Microsystems, TU Delft

Peter Steutel
Wb 1151606, L1173
Delft, Januari 4 2010
Biomechanical Engineering, 3ME, TU Delft

Table of Contents

Proceedings of IDETC/CIE 2010
ASME 2010 International Engineering Technical Conferences &Computers and Information in Engineering Conference
2010, XXXXXX

XXXXX

DESIGN OF A FULLY COMPLIANT UNDER-ACTUATED FINGER WITH A MONOLITHIC STRUCTURE AND DISTRIBUTED COMPLIANCE

Peter Steutel, Gert A. Kragten, Just L. Herder
Delft University of Technology
Faculty of Mechanical, Maritime and Materials Engineering,Department of BioMechanical Engineering
Mekelweg 2, 2628 CD Delft, The Netherlands
Email: J.L.herder@tudelft.nl

ABSTRACT

The majority of existing problems within conventional prosthetic fingers are related to the use of conventional rigid links and kinematic joints and to the lack of adaptability of the finger. In this paper these problems are solved by the design of a fully compliant under-actuated prosthetic finger. At first a basic structure was defined. Subsequently a Pseudo Rigid Body method was used for a type synthesis and rough dimensional analysis in order to determine the topology of the conceptual design. In order to evaluate the grasping behavior of the conceptual design, four mock-ups were created. Detailed dimensioning design was performed by semi automatic numerical analysis using a finite element method in which the conceptual design was used as an initial input. A prototype based on this final design was manufactured and experimentally evaluated. It was found that utilizing the concepts of under actuation and compliance solved the identified problems within conventional prosthetic fingers. As a result of the design process and the use of a predefined structure a fully compliant under-actuated finger with a monolithic structure and distributed compliance was obtained. In addition to the application field of prosthetics the design shows potential of being applied in the field of robotics and graspers.

Keywords: Prosthetics, Fingers, Under-actuation, Compliance, Monolithic structure

1 INTRODUCTION

Grasping and manipulating objects are daily activities for humans. Losing a hand due to a trauma is not only a traumatic experience but also influences the way of performing these activities. The use of a prosthetic device can be a solution to return a part of the function of the hand. However, a literature survey of conventional prosthetic fingers and graspers [1] showed two main problems related to the grasping capability and the mechanical design of the fingers.

The grasping capability of a prosthetic hand depends on the ability of the fingers to adapt to various object shapes and sizes and the required control effort. In conventional prosthetic fingers a low level of adaptation is related to a low amount of control effort and a high level of adaptation to a high amount of control effort. However a high level of adaptation with a low amount of control effort is desired. Problems related to the mechanical design are the result of using conventional rigid links and kinematic joints. Friction, backlash, wear, lubrication, fabrication costs, maintenance and weight are all problems related to this group. According to the author a solution for these problems could be obtained by designing a fully compliant under-actuated finger.

Under-Actuated mechanisms are mechanisms that have more degrees of freedom than number of actuators [2]. Within a prosthetic finger under-actuation can be achieved by utilizing an under-actuated mechanism in combination with objects blocking the phalanges. This can lead to a fully adaptable finger that is actuated by a single force. In [2-8] examples of prosthetic fingers and graspers with various types of under-actuation mechanisms (4-bar linkage mechanism [2], pulley mechanism [3-5] and seesaw mechanism [6,8]) can be found.

Compliant mechanisms transfer or transform motion, force or energy due to the deflection of flexible members [9]. These deflections can be obtained by utilizing the entire member (distributed compliance) or a small section of the member (lumped compliance). Within a finger compliant members can be used for some segments of the design (partially compliant) or

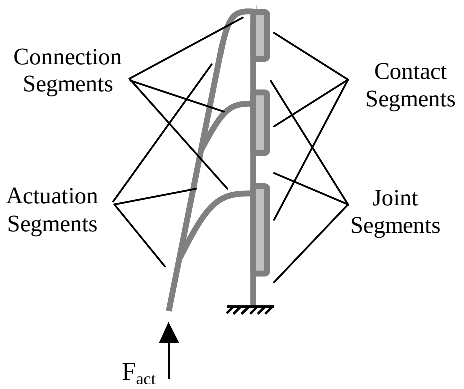

Figure 1 Schematic representation of the compliant basic structure with the four main variable segments indicated

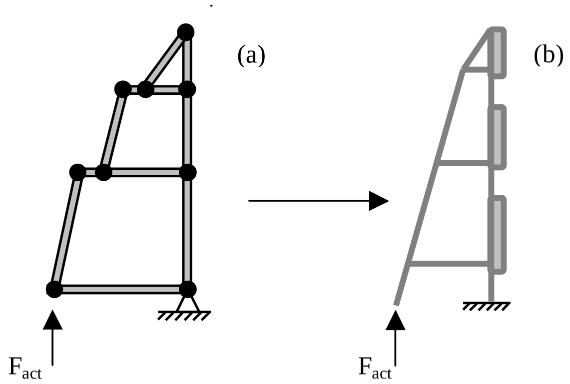

Figure 2 Schematic representation of the direct transformation of a conventional 4-bar rigid link under-actuated finger into its compliant form: (a) Rigid link model (b) Compliant model

for all the segments of the design (fully compliant). A fully compliant finger can result in a monolithic structure, which can reduce the fabrication costs and weight significantly [9]. Examples of conventional prosthetic fingers and graspers that are partially compliant can be found in [3, 10-12].

The goal of this article is to present the design of a fully compliant under-actuated finger with a monolithic structure and distributed compliance. Currently, such fully compliant under-actuated fingers with distributed compliance for prosthetic application do not exist. Although under-actuated mechanisms have been combined with compliant segments in fingers and graspers [3, 11-12], these mechanisms are only partially compliant. Examples of fully compliant under-actuated mechanisms, with a monolithic structure and lumped compliance, were only found within graspers [10, 13]. An example of a compliant under-actuated finger with a monolithic structure and distributed compliance however was not found.

A basic structure for a compliant under-actuated finger with a monolithic structure and distributed compliance is taken as a starting point for the design process (fig 1). This basic structure was the result of a literature survey, where the possibility of transforming various types of conventional under-actuated fingers into a monolithic compliant form was investigated [1]. The transformations were achieved by directly replacing the rigid links and joints of the conventional fingers with compliant segments having either flexible or stiff characteristics (fig 2). It was found that a basic structure of these compliant fingers consisted out of four main types of variable segments: Actuation segments, connection segments, contact segments and joint segments. The actual shape, size and number of used segments for a compliant under-actuated finger still has to be defined.

Starting with the basic structure as a starting concept, the structure of the paper is as follows; First the criteria for the design are presented. Second a conceptual design is obtained and evaluated by four mock-ups. Third a numerical analysis with a finite element method is executed which resulted in the final design. Finally a prototype of this final design was manufactured and evaluated experimentally.

2 DESIGN CRITERIA

The monolithic compliant under-actuated finger was designed with the intention to integrate it into a prosthetic hand in a later phase. The design should therefore incorporate anthropomorphic dimensions of the human finger including the following. The total length (distance form proximal joint to distal phalanx tip), the width (distance from proximal joint to actuation segment) and thickness were set at: 100 mm, 30 mm and 10mm respectively. Furthermore phalanx length ratios (proximal : middle : distal) of respectively 1 : 2/3 : 1/2 were desired. The maximum amount of rotation for each individual joint was set to 30 degrees. This results in a total deflection of 90 degrees of the distal phalanx and the maximal deflected orientation of the design. The transmission of the actuation force towards the contact forces, between the phalanges and grasped object, should be as high as possible. A good grasping behavior is achieved when no buckling phenomena occur in the entire range of deflection, during actuation. The maximum displacement of the actuation point, to achieve the maximal deflected orientation, was set to 50 mm due to the limited space within a prosthetic hand. In order to obtain a robust design the overall stiffness of the design has to be as high as possible. Distributed compliant members will be used to reduce the chance of high local stress concentrations. The stress in the segments should remain below the maximal yield strength of the used material. In order to obtain a monolithic structure, the design has to consist of a fully compliant structure.

3 CONCEPTUAL DESIGN

To design compliant mechanisms, several design methods have been developed in the literature. The approaches of these methods can be divided into three main categories [14]: Kinematic approach [9], Building block approach [15] and Structural optimization approach [16]. Within the kinematic approach, designs are obtained by focusing on the kinematic requirements of the design. The building block approach

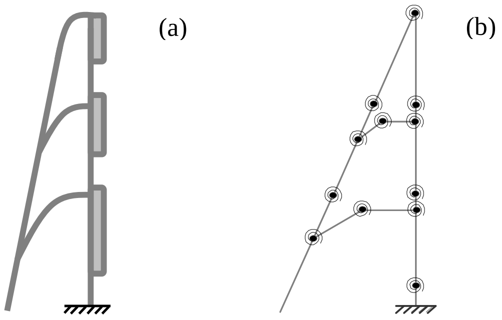

Figure 3 Typical example of transforming a compliant structure into its PRB model: (a) Compliant basic structure (b) PRB model basic structure

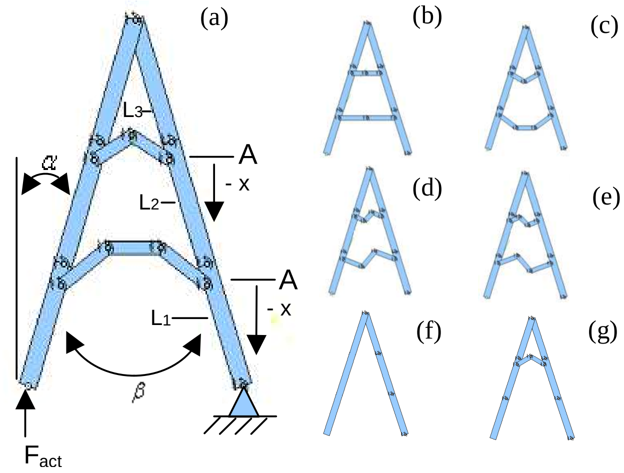

Figure 4 PRB models used in the simulation program during the type synthesis: (a) Basic model with variable parameters indicated and C-shaped connection (b) Straight connection (c) Reversed C-shape (d) S-shape (e) Reverse S-shape (f) One connection segment and one actuation segment (g) Two connection segments and three actuation segments

utilizes basic compliant segments (building blocks) by combining them into structures that can perform complex tasks. The Structural optimization approach obtains designs by means of an optimization procedure where an objective function is satisfied for a given set of parameters and constraints. Due to the fact that the design of the finger was based on the predefined basic structure and that the design criteria were based on kinematic requirements, a kinematical design method was used.

A design methodology within the kinematic approach group is the Pseudo Rigid Body method (PRB). In this method compliant segments are modeled as rigid segments connected by ideal joints and torsion springs [9]. With these models the deflection path and the force-deflection relationships of the compliant segments can be approximated.

The PRB method was utilized during the conceptual design phase by initially transforming the compliant structure into a PRB model (fig3). The PRB Model was used to determine the most promising conceptual design based on the design criteria. This was done in three steps. First, a Type Synthesis was executed in order to obtain the most promising topology for the conceptual design. Second the dimensions of the conceptual design were determined by means of a Dimensional Analysis. Third, four mock-ups (fig 8) were fabricated to evaluate the grasping behavior of the obtained conceptual design.

3.1 Type Synthesis

With the type synthesis the most promising topology (structure), based on the stated criteria, was determined by executing a topology synthesis and topology analysis. During the topology synthesis different topologies were obtained by identifying and varying a set of seven parameters (fig 4a-g).

1) The number of connection segments (n= 1, 2, 3)
2) Location connection segment (location A, A-x and A-2x with x = 7 mm)
3) The angle alpha of the actuation segment (alpha = 0^0 and alpha = 18^0)
4) Number of actuation segments (n= 1 and n= 3)
5) Top angle beta (beta = 22.5^0, 28^0 and 36^0)
6) Type of connection segment (Straight beam, C-shape, reverse C-shape, S-shape and reverse S-shape),
7) Lengths phalanges (1: L_1=L_2=L_3= 20mm, 2: L_1=30 mm L_2 = L_3 = 20 mm, 3: L_1 = 30 mm L_2 = 20 mm L_3 = 15 mm).

The effect of these parameters on the grasping behavior, the actuation displacement, the individual transmission ratios of the actuation force towards the contact forces and the transmission ratio of the actuation force towards the sum of the contact forces (input-output force relationship), was then analyzed during the topology analysis.

The topology analysis was executed with a simulation program (Working Model) in which a PRB model of the finger was built. For each identified parameter and specified range a simulation was executed. During each simulation the PRB models were actuated with a constant velocity resulting in a variable actuation force. Three fixed objects blocking the phalanges defined the grasping sequence (fig 5). The objects were placed such that the maximal deflected orientation was obtained at the end of a grasping sequence. The length of the actuation path was determined indirectly by the amount of time it takes for the distal phalanx to come in contact with the final object. The actuation force and contact forces exerted by the objects on the proximal and middle phalanx were determined directly by the Working Model program. To simplify the simulation process the PRB model of the basic structure were modeled symmetrical and the stiffness of the springs remained constant during each simulation.

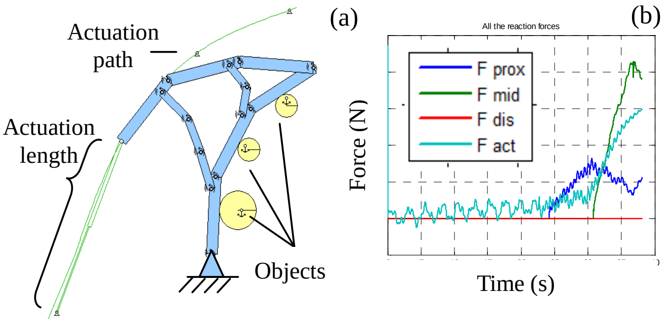

Figure 5 Typical presentation of the Working Model simulation results: (a) Final configuration of finger at the end of a simulation (b) Data output of the Actuation and Contact forces in a graph

The results of the type synthesis indicated that the most promising topology of the conceptual design will consist of three connection segments connected at the most distal point of each phalanx to increase the contact forces and off-axes stiffness of the structure. The actuation segment angle alpha will be set at approximately 18 degrees to reduce deflections of the actuation point. A combination of two flexible and three stiff segments will form the actuation segment to be able to achieve the maximal deflected orientation. The top angle beta will be as large as possible to achieve the highest ratio between the actuation force and contact forces. The proximal and middle connection segments will be S-shaped. Although the results of the C-shaped segment indicated higher individual transmission ratios between the actuation force and contact forces, the C-shaped segment increases buckling phenomena in the actuation segment. In addition, high local stress concentrations are expected due to large rotations in the connection point between the actuation segment and the connection segment, as in the straight connection segment. In order to obtain the highest input – output force ratio, the lengths of the proximal, middle and distal phalange will be 30 mm, 20 mm and 15 mm respectively according to the criteria.

As a result of the type synthesis a finger with three S-Shaped connection segments, two flexible and three stiff actuation segments under an angle of 18 degrees and lengths of the proximal, middle and distal phalanx of respectively 30 mm, 20 mm and 15 mm was chosen as the topology of the conceptual design (fig 6a).

3.2 Dimensional Design

In this section the unknown dimensions of the conceptual design were determined with a dimensional analysis. The length, thickness and rotation angle of each segment was determined by analyzing the segments individually, resulting in 14 segments (fig 6a).

The lengths of the segments were determined directly from the stated criteria and topology of the conceptual design. With these lengths a PRB model was built in order to determine the

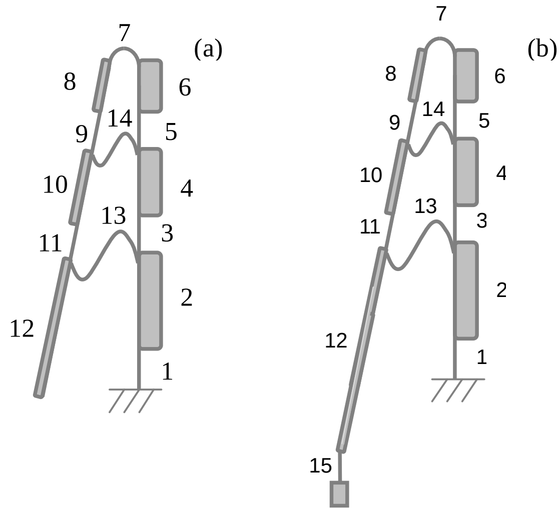

Figure 6 Schematic representations of the two conceptual designs with the individual segments indicated: (a) First conceptual design (b) Final second conceptual design

maximal amount of rotation of the segments using the Working Model program. The thickness of the segment depended on whether the segment had stiff or flexible characteristics. The segments: 2, 4, 6, 8, 10 and 12 of the conceptual design have stiff characteristics and segments 1, 3, 5, 7, 9, 11, 13 and 14 have flexible characteristics. The thickness of the stiff segments were selected merely on the fact that they may not deform. To determine the thickness of the flexible segments non-linear models were used. Assuming that the deformations of segments 1, 3, 5, 9 and 11 are initiated by a moment allowed the use of straight beam theory with an end moment [9]. For segments 7, 13 and 14 the theory of initially curved beams with an end force was applied [9]. Within each model the segment length and the maximum amount of rotation of the segment were used as input parameters. Varying the thickness of the segment will allow the determination of the required deflection force and resulting stresses inside the segment for a given length-rotation-thickness combination. Comparing these stresses with the maximum allowable stress of the used material will result in determining the maximal thickness. A safety factor of n=1.25 was used for the yield strength to allow a large number of loading cycles [17]. Five different types of materials were investigated, namely titanium, aluminum, stainless steel, plastic and nitinol. The obtained length-thickness results of the flexible segments were also checked on buckling, using the standard buckling and torsion formulae [18].

For the initially curved beam model the initial shape of the segment had to be defined and used as input. Due to the fact that only simple curved beams with a certain radius (Ri) could be modeled with this theory, segments 13 and 14 were modeled as two connected C-shaped beams (fig 7b). The rotation angels of the C-shape on the actuation segment side are smaller than

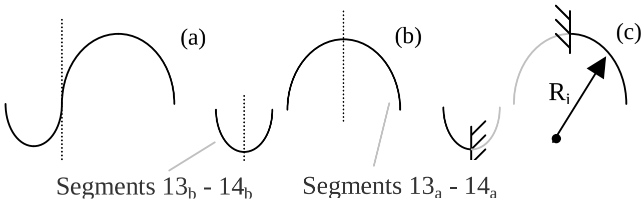

Figure 7 Modeling of the S-shaped connection segments: (a) Single segment (b) Two C-shaped segments (c) Four initially curved segments

the rotation angles of the C-shape on the phalanx side. This resulted in the use of two separate models (segments 13_a - 13_b and 14_a - 14_b). Assuming that each C-shaped segment has symmetrical properties, the C-shapes could be modeled as two curved segments each taking account for half the total deflection (fig7c). In order to achieve a connection segment with a uniform thickness the lengths of the two-modeled C-shapes will differ and the smallest thickness was used. Segment 7 was modeled as a single C-shaped segment.

As a result of the dimensional analysis the length, rotation angle and width of the individual segments of the conceptual design were obtained. These results are presented in table 1.

3.3 Mock-ups

Four mock-ups were created as a quick method to evaluate the grasping behavior of the conceptual design by executing simple grasping tasks. In each grasping task the finger was actuated, by applying a displacement, until the maximal deflected orientation was obtained. The mock-ups were created from plastic strips, which were glued together (fig 8 a-b) and from stainless steel sheets connected by small welding points (fig 8 c-d). Besides the S-shaped connection segments two mock-ups contained C-shaped connection segments. Simple grasping experiments with the plastic C-shaped mock-ups verified the buckling phenomena in segment 11 and local high stress concentrations as were identified during the topology analysis. The S-shaped mock-ups indicated promising grasping behavior, verifying the use of these connection segments in the conceptual design.

In the conceptual design phase the finger was actuated along a curved actuation path. Due to practical reasons and the lack of space inside a prosthetic device a vertical actuation path was introduced as an additional criterion. As a result of this criterion segment 12 was elongated and a flexible segment (15) was added to the conceptual design (fig 6b). These changes were implemented in the stainless steel mock-ups.

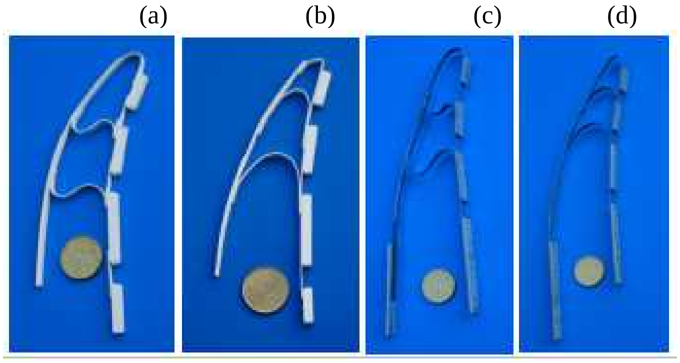

Figure 8 Four fabricated mock-ups with a 10 Eurocent coin used as a dimensional reference: (a) Plastic with S-shaped connection (b) Plastic with C-shaped connection (c) Stainless steel with S-shaped connection (d) Stainless steel with C-shaped connection

4 FINITE ELEMENT ANALYSIS

In order to analyze the interactions between the segments and the influence of these interactions on the deflections and stresses in the conceptual design, a numerical analysis was executed with a finite element method (FEM). With the FEM analysis the conceptual design will be refined towards a final design during two phases: Stress reduction and Dimensional refining.

4.1 FEM model

A commercially available program (ANSYS V11) was used to execute the FEM analysis. A FEM model of the conceptual design was built in order to perform grasping simulations. In each simulation the finger was actuated, by means of a displacement, until the maximal deflected orientation was obtained. The base of the finger was fixed in each direction and the actuation block was constraint horizontally resulting in a vertical displacement (fig 9). In order to achieve the maximal deflected orientation and to determine the related contact forces, three linear springs each fixed at one end and connected to the tip of a phalanx at the other end were used. Changing the dimensions of a segment subsequently resulted in changing the spring stiffness to acquire the maximal deflected orientation of the finger.

Table 1 Dimensions of the individual segments of the final conceptual design determined with the PRB method

Segment	**1**	**2**	**3**	**4**	**5**	**6**	**7**	**8**	**9**	**10**	**11**	**12**	**13**	**14**
Length (mm)	10	30	10	20	10	15	10	20	15	20	20	20	45	25
Rotation (degrees)	30	-	30	-	30	-	15	-	30	-	30	-	35	25
Thickness (mm)	0.22	3	0.22	3	0.22	3	0.58	1	0.33	1	0.44	1	0.12	0.14

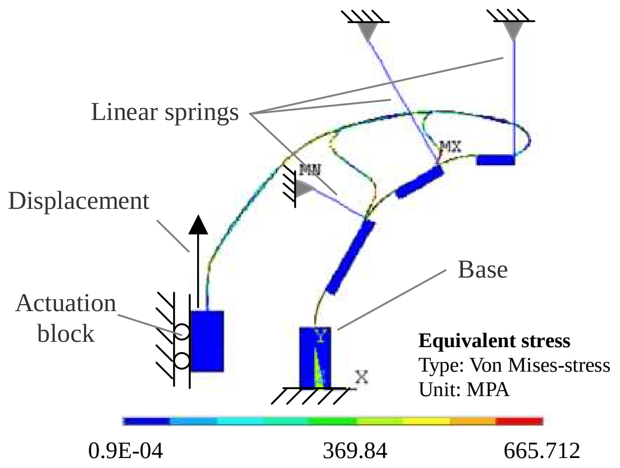

Figure 9 Von Mises-stress of the titanium Finite Element finger Model in the maximal deflected orientation in the ANSYS simulation environment

4.2 Final design

In the stress reduction phase the stresses in the segments that exceeded the defined maximum were reduced. In order to reduce the stress the flexibility of the segments should be increased by either reducing the thickness or increasing the length. Due to the fact that reducing the thickness has a larger negative influence on the torsion stiffness of the segments, the segments were initially elongated. The lengths of the segments were changed such that the criteria concerning the anthropomorphic dimensions of the design remained satisfied.

Initial FEM analysis indicated that the stresses in segments 1, 3, 5, 11, 13 and 14 exceeded the defined maximum. As a result of the stress reduction phase these segments were elongated from 10 to 13 mm (segments 1, 3 and 5), 20 to 27 mm, 45 to 48 mm and 25 to 26 mm respectively (table 2).

In the dimension refining phase the influence and relations of the segment stiffness on the grasping behavior, stress and phalanx contact forces were determined. This was done by means of a manual refining process in which the thickness of the segments was altered. The minimal thickness of the segments was set to 0.1 mm due to fabrication limitations. The identified relations were subjected to the stated criteria such that with a minimal amount of actuation displacement and actuation force the largest contact forces were obtained while the stresses remained below the defined maximum and good grasping behaviors were obtained.

During this phase the following relations were identified:

- Decreasing the stiffness of segments 3 and 5 improves the bending capabilities of these segments and decreases buckling phenomena in segments 9 and 11
- Increasing the stiffness of segments 9 and 11 hinders the bending capabilities of segments 5 and 3 and reduces the contact forces of segment 6 and 4. Decreasing their stiffness will increase the deflection (stress) of segments 14 and 13. Increasing the stiffness of segment 9 and decreasing the stiffness of segment 11 will increase buckling phenomena in segment 11.
- Segments 8, 10 and 12 were initially identified as stiff segments. However, allowing a certain degree of flexibility in these segments will reduce the deflections in segments 13 and 14, buckling phenomena in segment 11 and improves the bending capabilities of segments 3 and 5.
- Increasing the stiffness of segments 13 and 14 improves the bending capabilities of segments 3 and 5 and increases buckling phenomena in segment 11. Decreasing the stiffness will reduce the contact forces of segments 6 and 4. Increasing the stiffness of segment 13 and decreasing the stiffness of segment 14 will facilitate the bending capabilities of segments 3 and 5 and reduce the buckling phenomena in segment 11.
- Decreasing the stiffness of segment 15 will result in buckling phenomena in this segment. Increasing the stiffness will improve the bending capabilities of segments 1, 3 and 5, result in larger deformations of segments 13 and 14 and induce buckling phenomena in segment 9.
- Increasing the stiffness of segment 7 will increase buckling phenomena in segment 11.

As a result of the identified relations during the dimensional refining phase it was decided to modify the thickness of the following segments. The thickness of segments 3, 5, 8, 10 and 12 were reduced to improve the bending capabilities of segments 1, 3 and 5 and prevent buckling phenomena in segment 11. Connection segment 13 was increased and connection segment 14 decreased. The thickness of segments 7, 9 and 11 were reduced to prevent buckling phenomena in segment 11 while the thickness of segment 15 was not altered. The length and thickness of the individual segments of the final design are presented in table 2.

Table 2 Dimensions of the individual segments of the final design determined with the FEM analysis

Segment	**1**	**2**	**3**	**4**	**5**	**6**	**7**	**8**	**9**	**10**	**11**	**12**	**13**	**14**	**15**
Length (mm)	13	27	13	17	13	12	10	12	21	18	27	42	48	26	15
Thickness (mm)	0.21	3	0.19	3	0.18	3	0.3	0.63	0.26	0.63	0.37	0.63	0.13	0.11	0.25

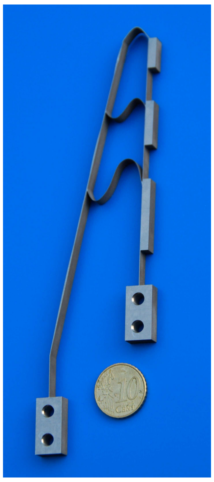

Figure 10 Titanium prototype of the fully compliant under-actuated finger with distributed compliance and a monolithic structure, 10 Eurocent coin used as a dimensional reference

5 PROTOTYPE

A prototype (fig 10) based on the final design was fabricated using electro discharge machining (EDM). EDM machining allows a high accuracy and is very applicable for thin walled constructions. Titanium Grade V (Ti6Al4V) was used as material due to its high strength to Young's modulus ratio, fabrication possibilities, predictable material properties and low susceptibility to creep. This material has a modulus of elasticity of 113.8 GPa, maximal yield strength of 827 MPa and a Poisson's ratio of 0.34 [9]. In order to increase the accuracy and reduce the chance of fracture of the thin-walled segments during fabrication the thickness of the prototype was reduced from 10 mm to 5 mm.

6 EXPERIMENTAL EVALUATION

In order to determine the required actuation displacement, related actuation force, resulting contact forces and joint deflections for a given closing sequence of the prototype an experimental evaluation was executed. The goal of this evaluation was to determine theses characteristics as well as identifying possible buckling phenomena in the prototype during two specific closing sequences: Free movement of the finger (experiment 1) and Maximal deflection of the finger (experiment 2). Besides determining the characteristics of the finger the results of the experiments were also compared with the FEM model in order to verify this model.

6.1 Experimental set-up

In order to perform the experiments a set-up was constructed (fig 11). The finger was fixed to the set-up at the base and placed in a horizontal plane to avoid the influence of gravity. The actuation block (fig 9) of the finger was connected to a linear rolling link mechanism to constraint the displacement

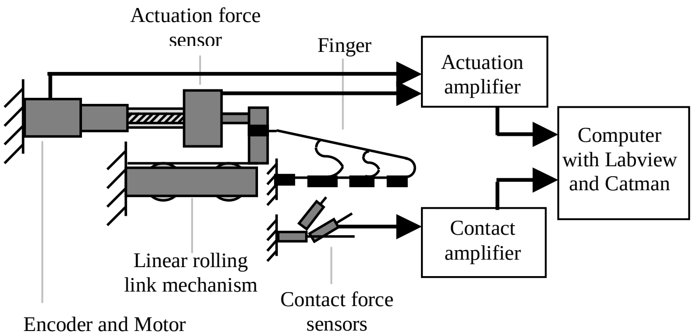

Figure 11 Top view of the experimental set-up with finger placed horizontally in its un-deflected position

into the horizontal direction. A Futek LSB 200 force sensor with a range of 100 N was used to measure the actuation forces and connected to the linear rolling link mechanism and the actuation block of the finger. The use of a force sensor with such a high range was due to the use of an existing set-up. A Maxon A-max 26, gear GP26 81:1 motor and Enc 22 encoder were connected to the actuation force sensor and used to actuate and measure the applied displacement. Three Scaime EP2 force sensors with a range of 20 N blocked and measured the contact forces in the phalanges. Two different amplifiers were used to increase the sensitivity of the force sensors. For the actuation force sensor a ICPDAS SG-3016 amplifier was used and for the three contact force sensors a HBM MGC+ 8 channel ML801 amplifier. All data was send to a computer and processed by two programs, LABVIEW for the encoder, motor and actuation force sensor and CATMAN for the three contact force sensors.

In the first experiment the free movement of the finger was evaluated in which the finger was actuated by applying a displacement until the proximal joint had bended for 30 degrees. During this experiment the encoder measured the applied displacement, the actuation force sensor the related actuation force and a protractor attached to the proximal phalanx the final rotation angle of the proximal joint.

In the second experiment the grasping behavior of the finger was evaluated in which the finger was actuated by applying a displacement until the maximal deflected orientation was obtained. In this case the bending of the joints was limited by 30 degrees. These limitations were obtained by the construction of mechanical stops connected to the three contact force sensors. The force sensors were positioned such that the normal forces of the phalanges were measured at the top of the distal and middle phalanx and at a distance of 5 mm from the top of the proximal phalanx. Due to the size of these force sensors the mechanical stop for the proximal phalanx could not be located at its top. During this experiment the encoder measured the applied displacement, the actuation force sensor the related actuation force, the three contact force sensors the contact forces and three protractors attached to the proximal, middle and distal phalanx the final rotation angles of the joints.

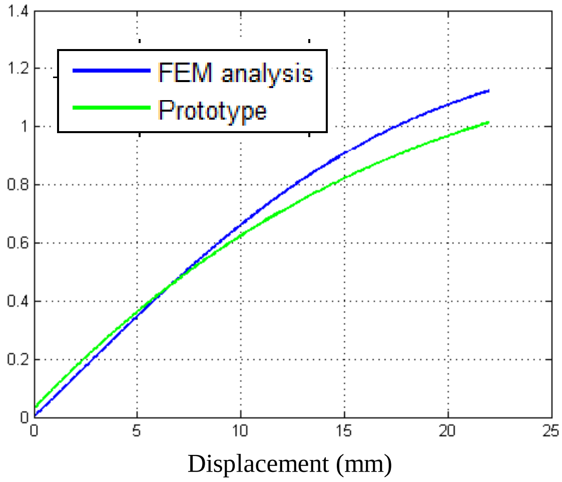

Figure 12 Force-displacement curve of the actuation point of experiment 1 of the Prototype and the FEM Model

Due to the different type of contact forces during a closing sequence between the FEM Analysis (constantly applied and increasing contact forces by the linear springs) and experiment 2 (suddenly applied contact forces by the objects) the actuation force-displacement curve could not be compared. The applied actuation force and contact forces when the finger is in the maximal deflected position however could be compared.

6.2 Data processing

Both experiments were executed 8 times with a sample rate of 25 samples/sec to increase the amount of data and the ability of reducing the noise. For each experiment all the data of the 8 experiments were combined in order to obtain a single data set. For the actuation force-displacement curve of experiment 1, a four-degree polynomial fit was used to average the actuation force and displacement data of this single data set and reduce the noise. For experiment 2 the final values of all the data were used. Because the finger was kept in its maximal deflected position for a few seconds, multiple data points of the final actuation and contact forces were measured. Averaging these data points resulted in the final averaged data set.

The linear actuator was theoretically frictionless. However the physical model indicated the presence of friction during a displacement. To eliminate the influence of this friction on the measured data, the friction of the linear actuator during a displacement of 45 mm was determined and reduced from the measured data of the actuation force sensor.

6.3 Experimental results

The force-displacement curves of the actuation point during experiment 1 of both the prototype and the FEM analysis are presented in figure 12. With an applied actuation displacement of 22 mm, the proximal phalanx has bended for 30 degrees in both the FEM analysis and experiment. Actuation forces of respectively 1.12 N and 1.03 N were required to obtain these deflections.

Table 3 Applied actuation displacement (Y_{act}) associated actuation force (F_{act}) and resulting phalanx rotation angles and contact forces (F_{con}) of experiment 2 of the Prototype and the FEM Model

	Y_{act} (mm)	F_{act} (N)	Rotation angle Prox:Mid:Dist phalanx (deg)	F_{con} Prox:Mid:Dist phalanx (N)
FEM Analysis	45	2.17	30:30:30	0.86:0.37:0.29
Prototype	45	1.98	30:30:30	0.79:0.37:0.32

The results of experiment 2 are presented in table 3. The applied displacement, associated actuation force, resulting rotation angles and contact forces of the phalanges of the prototype and the FEM analysis are given. In both cases all three joints had bended for 30 degrees with an applied actuation displacement of 45 mm. The required actuation forces and resulting contact forces (proximal, middle and distal phalanx) were respectively 2.17, 0.86, 0.37 and 0.29 N for the FEM Analysis and 1.98, 0.79, 0.37 and 0.32 N for the prototype.

The closing sequence of the finger during the maximal deflection experiment indicated a behavior as stated in the criteria. No buckling phenomena were observed during a closing sequence towards the maximal deflected orientation. In figure 13 the closing sequence of the finger during the second experiment is presented.

7 DISCUSSION

This paper presented the design of an under-actuated compliant finger with a monolithic structure and distributed compliance based on a predefined basic structure. As a result of the executed design method a prototype and FEM model were obtained. The prototype of the finger meets the stated criteria concerning the anthropomorphic dimensions and is capable of reaching the maximal deflected orientation without buckling phenomena or plastic deformations of the segments. The under-actuation capabilities of the finger resulted in an adaptable finger actuated by a small single force. The amount of adaptability was however limited to a maximum deflection of 30 degrees for each joint. The obtained monolithic structure resulted in a lightweight design (15.1 grams) that requires no assembly, maintenance or lubrication and is not influenced by aspects such as friction and backlash. Overall a new type of an under-actuated compliant finger was obtained which shows promising characteristics and capabilities for the field of prosthetics.

The required force to freely actuate the finger until a rotation of 30 degrees of the proximal joint was reached, was compared with the FEM model. A maximal difference of 10% was found at the end of the force-deflection trajectory. This difference can be explained by inaccuracies between the FEM model and the prototype due to fabrication techniques, differences between the theoretical and used material properties and the presence of some degree of flexibility in the experimental set-up. The maximal difference in the contact forces during experiment 2 was 9%. This difference can be explained by the presence of some degree of flexibility in the experimental set-up and the difficulty of measuring the exact rotation angles. In addition to these differences, small measurement errors were introduced in the data due to the use of the actuation force sensor, which had a relatively poor resolution and the use of a polynomial fit in order to average the data. Despite these errors the total differences are relatively small which allows the conclusion that the created FEM model is a valid tool capable of giving good indications and predictions of the grasping behavior of the prototype.

The finger was initially designed for the field of prosthetics. However the design and design process, utilizing the basic structure, show such potential that these can even be used in other fields such as robotics and graspers due to comparable design and grasping requirements.

The stress in the segments determined with the PRB method and FEM Analysis was different due to two reasons. First the assumption that only moments act on the segment and that the segment has a free movable tip is not an exact representation of the situation. In the real case both a moment as a force act on the segment and the tip follows a curved path depending on the type of grasped object. Instead of the entire segment only a part of the segment will take account for the deflection resulting in higher stresses. Secondly filets were incorporated in the design during the FEM Analysis at the connections of the joint segments with the contact segments and at the connections of the connection segments with the contact and actuation segments. This was done for fabrication reasons and in order to prevent high local stress concentrations in these points. As a result the stiffness of these segments increased.

The final design was obtained using linear springs in the simulations of the FEM analysis to represent contact forces on the phalanges. These springs limited the ability of creating large contact forces in combination with obtaining the maximal deflected orientation. Attempts of defining contact surfaces in the FEM analysis were not successful due to non-converging simulations and surface penetrations. More realistic simulations can be executed when contact surfaces are used to block the phalanges. Future investigation should be executed on implementing contact surfaces in ANSYS. Using contact surfaces will also simplify the execution of an optimization procedure within ANSYS, which can result in obtaining the best design for a given objective function that satisfies a given set of parameters and constraints.

The required actuation force and subsequently the associated contact forces are relatively low. This is due to relatively low overall stiffness of the design. For the actuation force this is an advantage however, for the robustness of the design it is a disadvantage. In order to increase the robustness the overall stiffness has to be increased. Additional joint segments parallel to the single joint segment in the current design can achieve this. To achieve similar bending capabilities of a single joint the length of the parallel joint segments will have to vary. Increasing the stiffness will subsequently increase the energy storage in the compliant segments, which will result in an increase of the actuation force and distortion of the input-output relationship [19]. A possible solution for the energy storage is implementing the concept of statically balancing in the design [20].

The used S-shaped connection segment in the design has both compression and tension spring characteristics, which is beneficial for the behavior of the finger. The compression spring characteristics are utilized when objects block the phalanges resulting in an increase of contact forces between the phalanges and grasped objects. The tension spring characteristics are utilized when the proximal phalanx is blocked and the grasping sequence continues. From this point the actuation segments continue deviating while the phalanx remains fixed. Buckling phenomena of the actuation segments are reduced due to the limited extension capabilities of the connection segment. Subsequently a rotating sequence of the actuation segments around the proximal phalanx is initiated which facilitates the bending possibilities of the middle and distal joint. Because the deviations in the connection segments are high, they have to be very flexible to prevent plastic deformation or even fracture. However, when the connection segments become too flexible the overall stiffness of the design will reduce as will the spring characteristics. In order to obtain S-shaped connection segments with high stiffness and capable of large rotation angles, while maintaining the spring characteristics, the segments could be pre-stressed. The initially stored energy in the pre-stressed segments could be statically

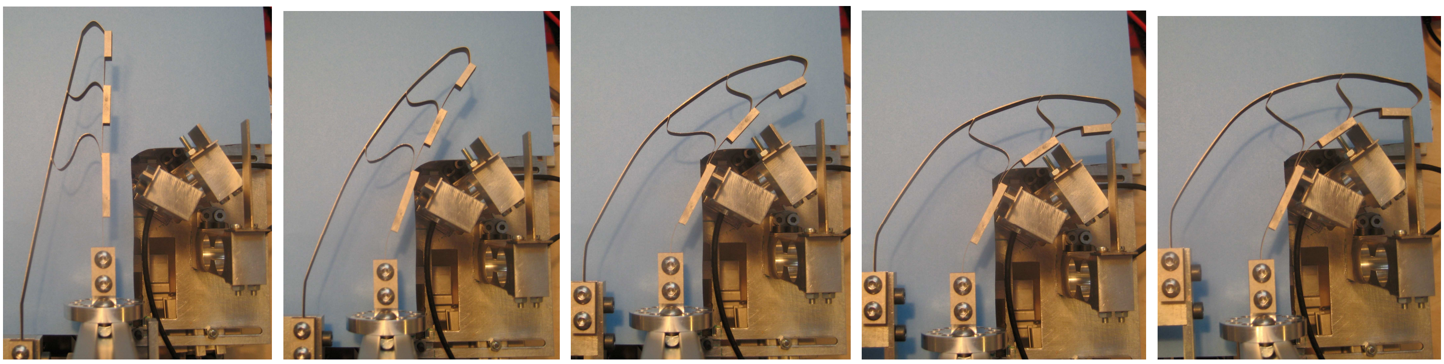

Figure 13 Closing sequence of the titanium prototype form its original un-deflected orientation to the maximal deflected orientation during experiment 2

balanced in order to reduce the influence of this energy on the input-output relationship. Future investigations have to be executed on the influence and possibility of pre-stressing segments in monolithic structures.

The actuation path has a large influence on the actuation and contact force relationship. A vertical actuation path as is used in the final is not the most optimal path. Future investigations should be executed in order to determine the most optimum actuation path and the possibility of implementing this path in the design.

8 CONCLUSION

This paper proposes an under-actuated compliant finger with a monolithic structure and distributed compliance based on a predefined basic structure. It was found that combining the concepts of under-actuation and fully distributed compliance in a finger was successful. The obtained monolithic structure resulted in a lightweight design (15.1 grams) that requires no maintenance or lubrication and is not influenced by aspects such as friction and backlash. Furthermore the obtained design requires a small single actuation force (1.98 N) to acquire the maximal deflected orientation in which all three joints have rotated for 30 degrees without the presence of buckling phenomena and plastic deformations. The design process of utilizing the predefined basic structure and executing a Pseudo Rigid Body analysis followed by a Finite Element Analysis has resulted in a working prototype and a validated FEM model.

For the first time a compliant under-actuated finger was designed with a monolithic structure and distributed compliance. Furthermore the designed finger shows such promising characteristics; under-actuated, small single actuation force, monolithic structure, lightweight and adaptable, that it has great potential for further development in the field of prosthetics, robotics and graspers.

REFERENCES

[1] Steutel, P. (2009), 'An overview window for the conceptual design of a prosthetic finger', Literature survey, Delft University of Technology, Delft, The Netherlands

[2] Laliberte, T., Birglen, L. and Gosselin, C. M. (2002), 'Underactuation in robotic grasping hands', *Machine intelligence & Robotic Control*, November 2002, Vol4, No. 3

[3] Dollar, A.M. and Howe, R.D. (2007), 'The SDM hand as a prosthetic terminal device: A feasibility study', *Proceedings of the 2007 IEEE 10th International Conference on Rehabilitation Robotics*, Noordwijk, The Netherlands, June 12-15, 2007

[4] Carrozza, M. C., Suppo, C., Sebastiani, F., Massa, B., Vecchi, F., Lazzarini, R., Cutkosky, M.R. And Dario, P. (2004), 'The spring hand: Development of a self adaptive prosthesis for restoring natural grasping', *Autonomous Robots*, Vol. 16, pp. 125-141

[5] Hirose, S. and Umetani, Y. (1978), 'The development of Soft Gripper for the versatile robot hand', *Mechanism and Machine Theory*, Vol. 13, pp. 351-359

[6] Fukaya, N., Toyama, S., Asfour, T. And Dillmann, R. (2000), 'Design of the TUAT/Karlsruhe humanoid robot', *Proceedings of the 2000 IEEE/RSJ, International Conference on Intelligent Robots and Systems*

[7] Montambault, S. and C. M. Gosselin (2001), C. M., 'Analysis of Underactuated Mechanical Grippers', *Journal of Mechanical Design*, Vol. 123, September, 2001

[8] Kyberd, P. J. and Pons, J. L. (2003), 'A comparison of the oxford and manus intelligent hand prostheses', *Proceedings of the 2003 IEEE International Conference on Robotics & Automation*, Taipei, Taiwan, September 14-19, 2003

[9] Howell, L. L. (2001), 'Compliant Mechanisms', John Wiley & Sons

[10] Boudreault, E. and Gosselin, C. M. (2006), 'Design of Sub-Centimetre Underactuated Compliant Grippers', *Proceedings of International Design Engineering Technical Conference & Computers and information Conference*, Philadelphia, Pennsylvania, USA, September, 2006

[11] Lotti, F., Tiezzi, P., Vassura, G., Biagotti, L. And Melchiorri, C. (2004), 'UBH 3: an anthropomorphic hand with simplified endo-skeletal structure and soft continuous fingerpads', *Proceedings of the 2004 IEEE International Conference on* Robotics & Automation, New Orleans, LA, USA, April, 2004

[12] Tsai, Y. C., Lei, S. H. And Sudin, H. (2005), 'Design and analysis of planar compliant micro gripper based on kinematic approach', *Journal of Micromechanics and Microengineering*, Vol. 15, pp.143-156

[13] Doria, M. and Birglen, L., 'Design of an Underactuated Compliant Gripper for Surgery Using Nitinol', *Journal of Medical Devices*, March, 2009, Vol. 3

[14] Gallego, J. A. and Herder, J.L. (2009), 'Synthesis methods in compliant mechansisms: an overview', *Proceedings of the ASME 2009 International Design Engineering Technical Conference & Computers and information Conference*, San Diego, USA, September, 2009

[17] Stikeleather, L.F., 'Column buckling', www.bae.ncsu.edu/www3/pe/2009/materials/ii-b/ii-b.ppt (retrieved, 26-11-2009)

[18] Department of Aerospace engineering, 'Torsion of Non-Circular Bars', http://www.ae.msstate.edu/~masoud/Teaching/SA2/chA6.4_text.html (retrieved, 26-11-2009)

[19] Salamon, B.A. and Middha, A. (1998), 'An introduction to Mechanical advantage in compliant mechanisms', *Journal of Mechanical Design*, Vol 120, pp 311-316, June

[20] Herder, J.L. (2001), 'Energy-free Systems; Theory, conception and design of statically balanced spring mechanisms', PhD Thesis, Delft University of Technology, ISBN 90-370-0192-0, chapter 3

Appendix [A]

Type synthesis

The simulations of the type synthesis were executed with the simulation program: Working Model. This program allows the user to built rigid body structures and investigate their kinematical and dynamical working capabilities on a very basic level. Connecting two rigid structures with a kinematical hinge and a rotational spring will resemble the compliant segments (PRB model). Altering the stiffness of the rotational spring will alter the stiffness of the 'compliant' segment. A pneumatic rod is used to apply the necessarily actuation forces in the simulations. This rod resembles a constant actuation velocity from which the required actuation forces can be derived. The objects that where grasped are resembled by circles placed on the side of the phalanges and fixed to their position. By fixing the grasped objects, the contact forces and the kinematics (closing sequence) of the model can be investigated. During each simulation the finger was actuated until the maximal deflected orientation of the finger was obtained (distal phalanx making contact with an object).

The basic structure (fig 1a) determined during a literature survey of the author is used an initial structure for the conceptual design phase. This structure was transformed into a PRB model (fig 1b) that will be used in the simulations.

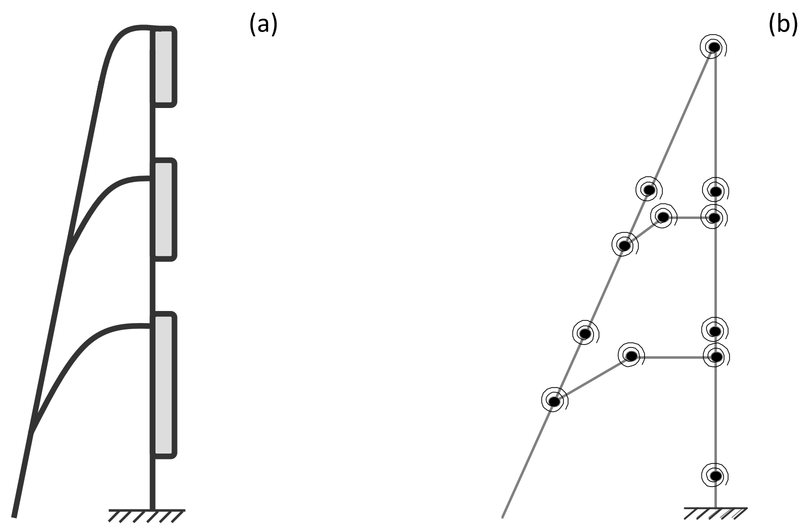

Figure 1: a) Basic structure, b) PRB model of basic structure

The PRB model used in the simulations is modeled as a symmetrical structure. The orientation and length of the actuation elements and phalanxes will therefore be equal. The difference in stiffness between the actuation and phalanx side is realized by using different stiffness values for the springs in the joints.

Variable parameters:
The following parameters were altered in order to investigate their influence on the kinematical properties and determine the most promising topology.

- The number of connection segments (n= 1, 2, 3)
- Location connection segment (location A, A-x and A-2x with x = 7 mm)
- The angle alpha of the actuation segment (alpha = 0^0 and alpha = 18^0)
- Number of actuation segments (n= 1 and n= 3)
- Top angle beta (beta = 22.5^0, 28^0 and 36^0)
- Type of connection segment (Straight beam, C-shape, reverse C-shape, S-shape and reverse S-shape),
- Lengths phalanxes (1: L1=L2=L3= 20mm, 2: L1=30 mm L2 = L3 = 20 mm, 3: L1 = 30 mm L2 = 20 mm L3 = 15 mm).

Fixed parameters:
Fixed parameters as described above are:

- Actuation path
- Actuation velocity
- Location objects
- Stiffness springs

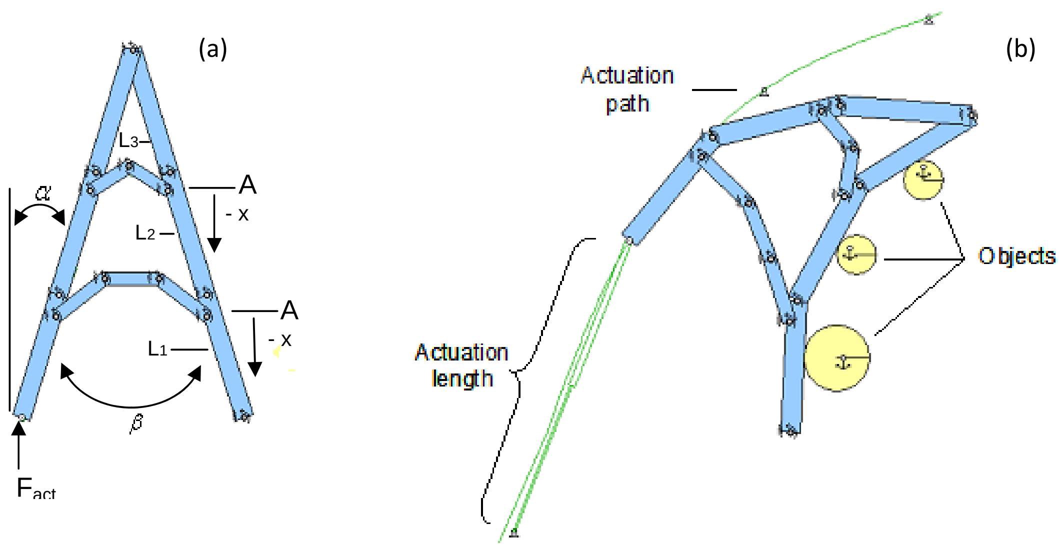

Figure 2: a) Un-deformed PRB model with variable parameters, b) Deformed PRB model in simulation environment

Performance criteria:
Judging the data results on the following performance criteria will do comparing the simulations:

- Actuation path
- Actuation force
- Contact forces

A good performance is stated as the smallest actuation path and the highest possible ratio between the actuation force and contact forces in which the actuation force should be low and the contact forces high. The topology should also be able to reach the maximal deflected orientation (each joint rotated for 30 degrees) without phenomena such as buckling arising during the grasping sequence.

First simulation phase

The number of connections elements, varying from one to three, is the first parameter that was investigated. In figures 3 a-c the used PRB models during the simulations are shown.

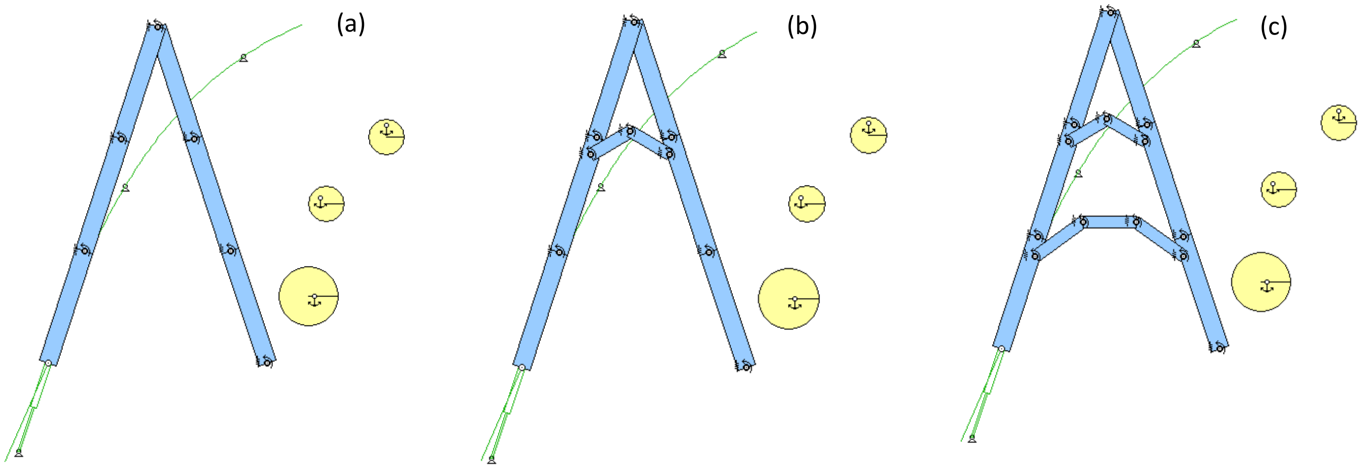

Figure 3: PRB models a) one connection element, b) Two connection elements, c) Three connection elements

Second simulation phase

The influence of the location of the connection segments in respect the centre of the phalanxes is the second parameter that was investigated. Three different locations were investigated, the top position A, middle position (A- X) and bottom position (A- 2X) with X = 7mm. In figures 4 a-c the used PRB models used for the simulations are shown.

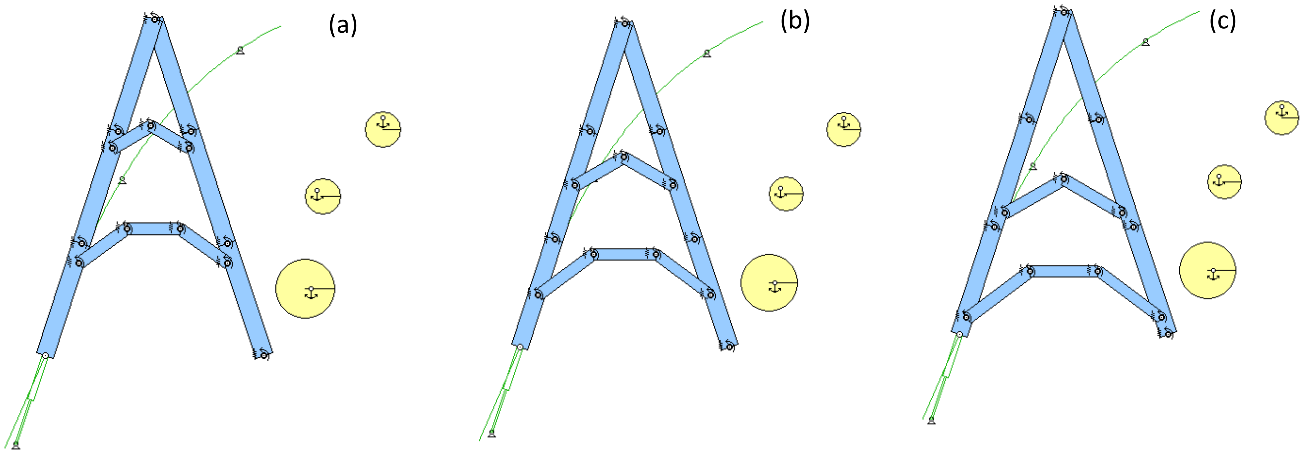

Figure 4: PRB models a) Connection at point A, b) Connection point A-x, c) Connection point A-2x

Third simulation phase

The third parameter investigated was the angle alpha. The orientation of the actuation segment and phalanxes is changed in respect to the vertical plane. Two positions were investigated a completely vertical position (alpha $=0^0$) and a position with alpha $= 18^0$. In figures 5 a-b the used PRB models during the simulations are shown.

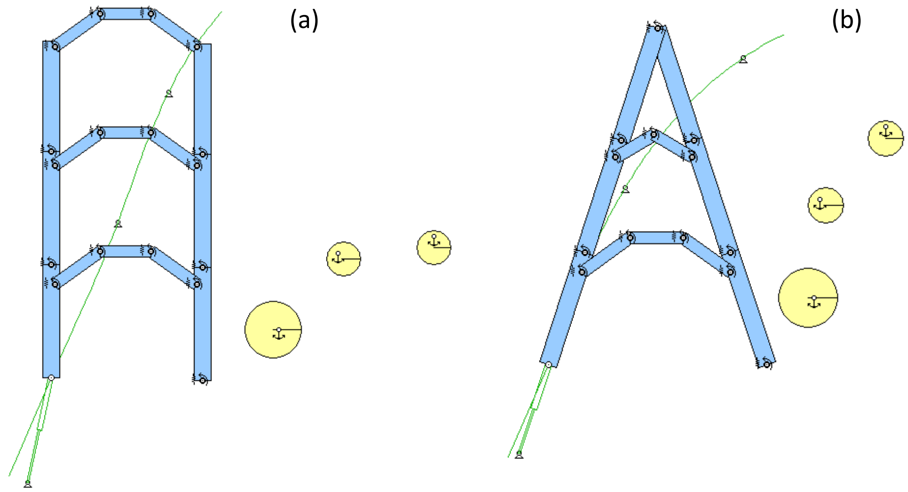

Figure 5: PRB models a) Actuation segment angle alpha = 0, b) Actuation segment angle alpha = 18

Fourth simulation phase

Whether the actuation segment should have stiff characteristics (1 segment) or a combination between stiff and flexible characteristics (3 segments) is investigated by the fourth parameter. The two PRB models used for the simulations are shown in figures 6 a-b.

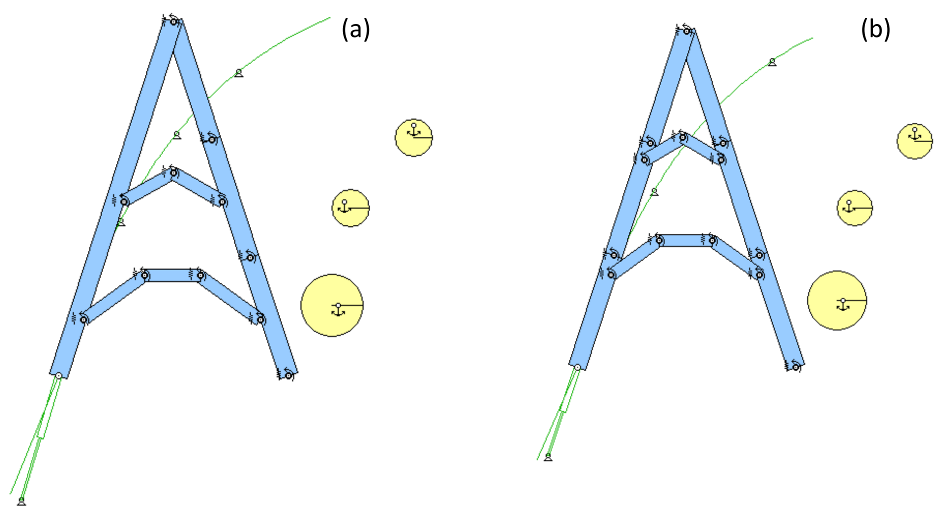

Figure 6: PRB models a) One actuation segment, b) Three actuation segments

Fifth simulation phase

The angle between the actuation segment and the distal phalanx (angle beta), determines the maximum width of the finger and the lengths of the connection segments. The influence of decreasing this angle is investigated with three simulations of which the used PRB models are shown in figures 7 a-c.

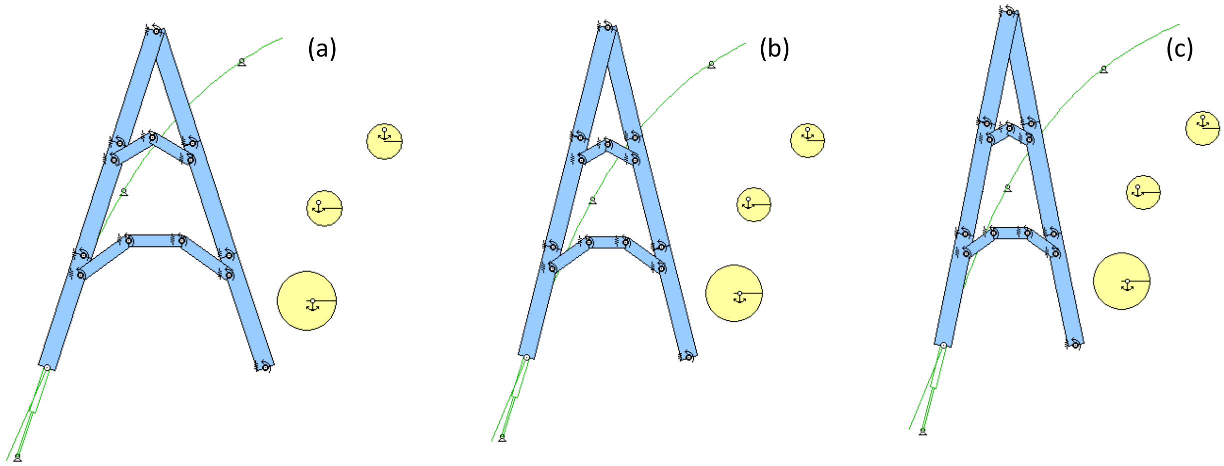

Figure 7: PRB models a) Angle beta = 22.5 degrees, b) Angel beta = 28 degrees, c) Angle beta =36 degrees

Sixth simulation phase

One of the design criteria stated the desire of achieving an anthropomorphic design. This implies that the lengths of the phalanxes should be un-equal. Increasing the length of the proximal phalanx and decreasing the length of the distal phalanx will result in a realization of this criterion. Three PRB models used to simulate and determine the influence of changing the dimensions of the phalanxes are shown in figures 8 a-c.

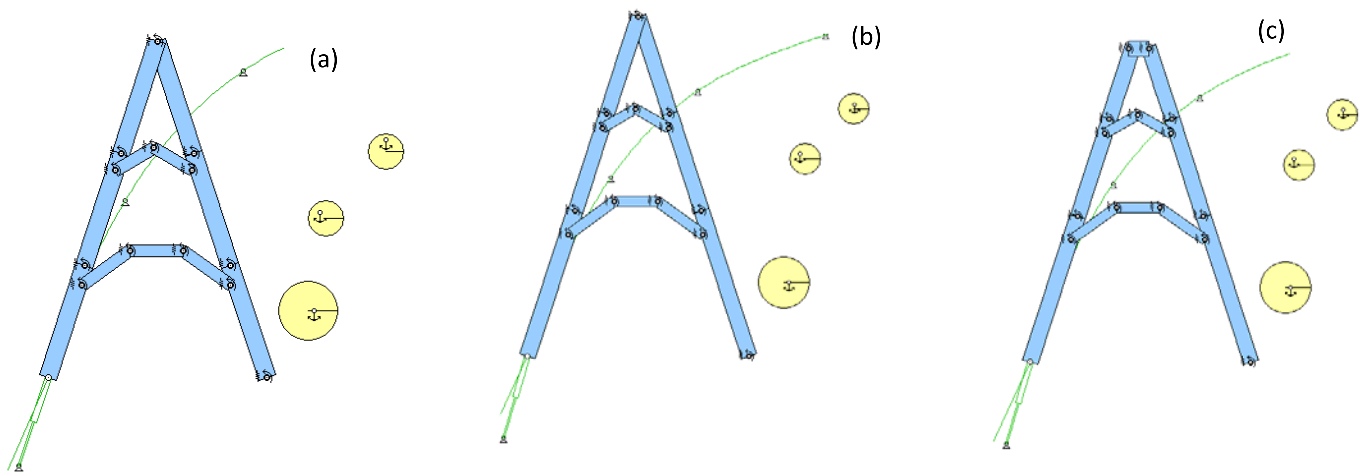

Figure 8: PRB models a) Phalange lengths L1=L2=L3= 20 mm, b) Phalange lengths L1= 30 mm and L2=L3= 20 mm, c) Phalange lengths L1= 30 mm L2=20 mm and L3 =15 mm

Seventh simulation phase

Three different types of connection segments were investigated. A straight segment, C-shaped segment and a S-shaped segment. Both the C-shaped and S-shaped segments were also mirrored around their horizontal axes, resulting in five different simulations. The PRB models of the simulations are shown in figures 9 a-e.

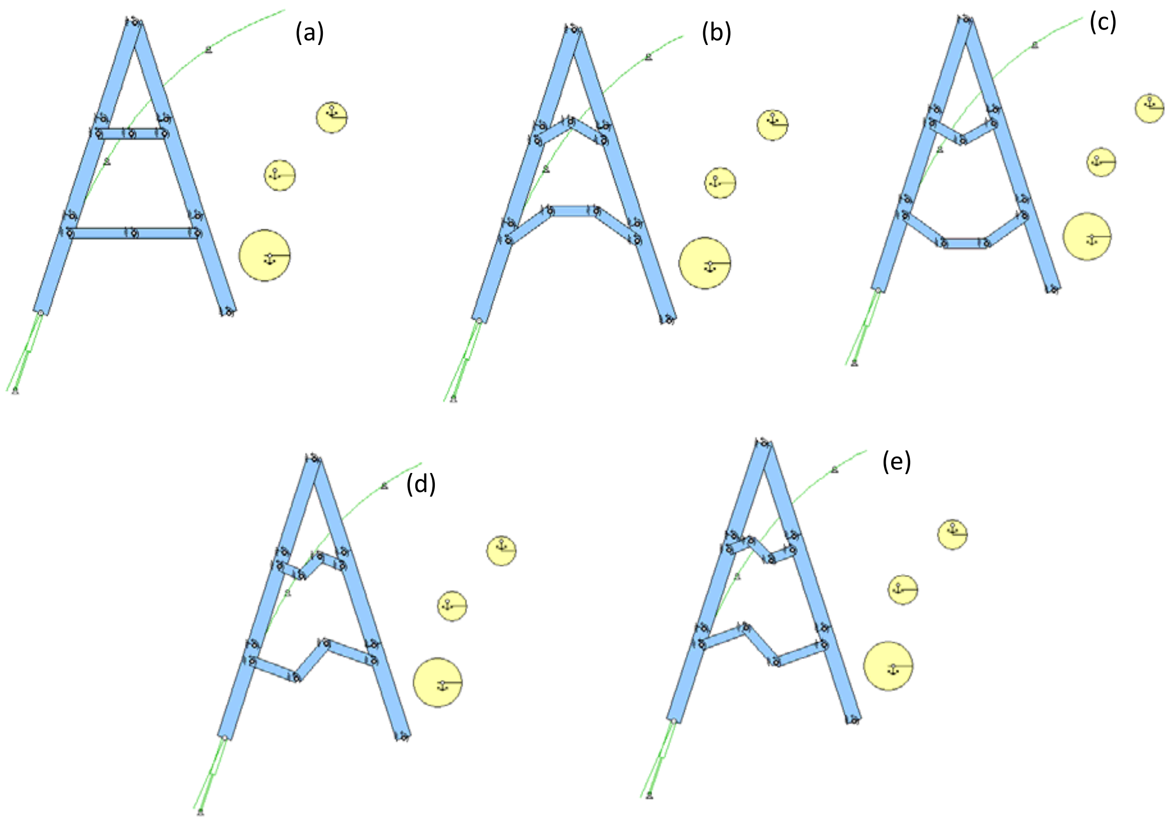

Figure 9: PRB models a) Straight connection segment, b) C-shaped connection segment, c) Reverse C-shaped connection segment, d) S-shaped connection segment, e) Reverse S-shaped connection segment

Results

The actuation force, reaction forces and rotation angles were measured continuously during a simulation by the working model program. The results for each simulation were analyzed using two plots, one containing the rotation angle of the distal phalanx and one containing the actuation and reaction forces. These plots will only be shown for the first simulation, the results of the other simulations will be presented in tables. In these tables the actuation time (time when distal phalanx makes contact with the final object) and the maximal actuation and reaction forces are presented. Identifying the most promising topology will be achieved by comparing these results and by analyzing the closing sequence of each simulation.

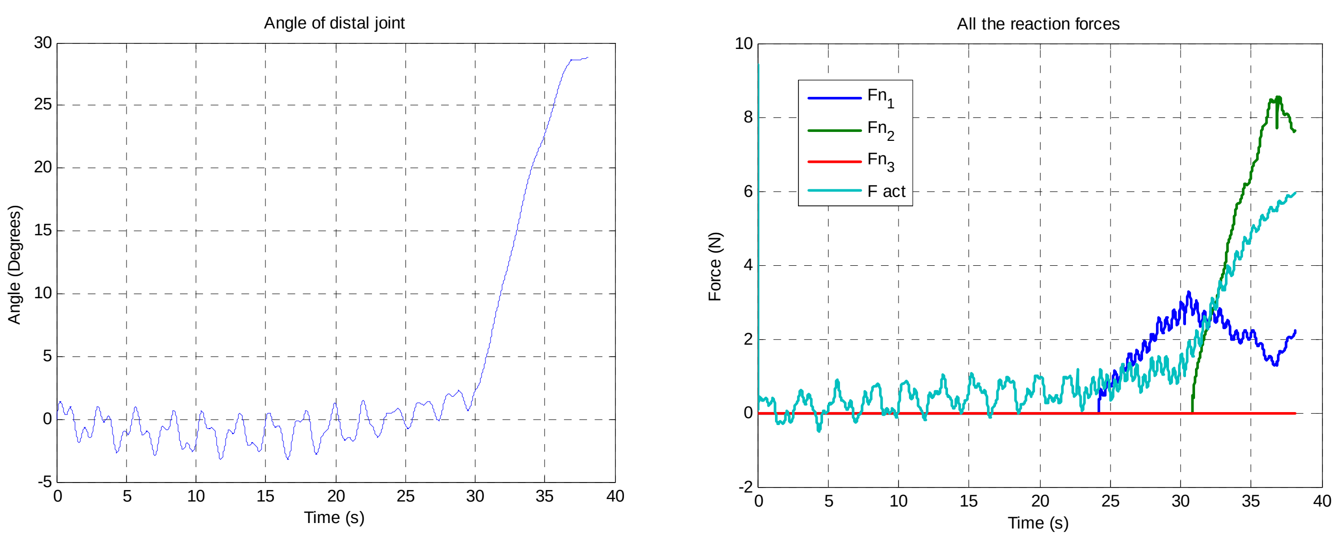

Figure 10: Plots of the results, a) Angle of distal phalanx, b) Actuation and reaction Forces

First simulation phase

Table 1: Results of the first simulation phase

Simulation Parameters	One connection element (1a)	Two connection elements (1b)	Three connection elements (1c)
T (sec)	38.1200	39.6400	38.7000
F_actuation (N)	5.9460	9.2860	20.8280
F_reaction_proximal (N)	3.2840	4.2890	25.2200
F_reaction middle (N)	8.5550	14.2850	23.8950
F_reaction_distal (N)	0	0	0

Second simulation phase

Table 2: Results of the second simulation phase

Simulation Parameters	Connection point A (1c)	Connection point A-x (2a)	Connection point A-2x (2b)
T (sec)	38.7000	37.9000	37.6200
F_actuation (N)	20.8280	10.9840	10.4220
F_reaction_proximal (N)	25.2200	10.8200	9.9960
F_reaction middle (N)	23.8950	14.3060	11.1340
F_reaction_distal (N)	0	0	0

Third simulation phase

Table 3: Results of the third simulation phase

Simulation Parameters	Angle alpha = 0^0 (3)	Angle alpha = 18^0 (1c)
T (sec)	46.8600	38.7000
F_actuation (N)	10.1420	20.8280
F_reaction_proximal (N)	10.3300	25.2200
F_reaction middle (N)	19.8470	23.8950
F_reaction_distal (N)	0	0

Fourth simulation phase

Table 4: Results of the fourth simulation phase

Simulation Parameters	One actuation segment (4)	Three actuation segments (1c)
T (sec)	33.1400	38.7000
F_actuation (N)	36.2360	20.8280
F_reaction_proximal (N)	36.6870	25.2200
F_reaction middle (N)	52.0460	23.8950
F_reaction_distal (N)	0	0

Fifth simulation phase

Table 5: Results of the fifth simulation phase

Simulation Parameters	Angle beta = 36^0 (1c)	Angle beta = 28^0 (5a)	Angle beta = 22.5^0 (5b)
T (sec)	38.7000	30.2200	23.3600
F_actuation (N)	20.8280	23.9730	38.9640
F_reaction_proximal (N)	25.2200	21.4120	24.2790
F_reaction middle (N)	23.8950	20.8240	28.6550
F_reaction_distal (N)	0	0	0

Sixth simulation phase

Table 6: Results of the sixth simulation phase

Simulation Parameters	Phalanx lengths L1=L2=L3= 20 mm (1c)	Phalanx lengths L1= 30 mm and L2=L3= 20 mm (6a)	Phalanx lengths L1= 30 mm L2= 20 mm and L3= 15 mm (6b)
T (sec)	38.7000	40.3400	41.1000
F_actuation (N)	20.8280	21.6680	22.3460
F_reaction_proximal (N)	25.2200	16.6780	16.9740
F_reaction middle (N)	23.8950	24.5370	25.9400
F_reaction_distal (N)	0	0	0

Seventh simulation phase

Table 7: Results of the seventh phase

Simulation Parameters	Straight connection element (7a)	C-shaped connection element (1c)	Reverse C-shaped connection element (7c)	S-shaped connection element (7d)	Reverse S-shaped connection element (7e)
Time (sec)	37.8200	38.7000	37.8800	38.3000	37.5200
F_actuation (N)	17.0590	20.8280	15.9970	16.4460	16.0520
F_reaction_proximal (N)	18.1250	25.2200	12.0050	19.5970	13.5220
F_reaction middle (N)	24.2360	23.8950	21.1100	19.5340	20.4530
F_reaction_distal (N)	0	0	0	0	0

Conclusions

The results of the various simulations were analyzed by comparing the values and determine the individual ratios between the actuation force and the reaction forces (F actuation: F proximal: F middle). The closing sequences of the simulations were also investigated on buckling phenomena and the ability of realizing the maximal deflected orientation

Table 8a: Overview of the result of the first four simulation phases with the maximum time and force ratio's

Simulation Parameters	**1a**	**1b**	**1c**	**2a**	**2b**	**3**	**4**
Time (s)	38.12	39.64	37.82	37.90	37.62	46.86	33.14
Force ratio's	1: 0.55:1.44	1:0.46:1.54	1:1.21:1.15	1:0.99:1.3	1:0.96:1.1	1:1.02:1.96	1:1.01:1.44

Table 8b: Overview of the results of the last three simulation phases with the maximum time and force ratio's

Simulation Parameters	**5a**	**5b**	**6a**	**6b**	**7a**	**7c**	**7d**	**7e**
Time (s)	30.22	23.36	40.340	41.10	38.70	37.88	38.30	37.52
Force ratio's	1:0.89:0.87	1:0.62:0.74	1:0.77:1.13	1:0.76:1.16	1:1.06:1.42	1:0.75:1.32	1:1.19:1.19	1:0.84:1.27

The results of the type synthesis indicated that the most promising topology of the conceptual design will consist of three connection segments connected at the most distal point of each phalanx to increase the contact forces and off-axes stiffness of the structure. The actuation segment angle alpha will be set at approximately 18 degrees to reduce deflections of the actuation segment. It consists of multiple flexible segments to achieve the maximal deflected orientation. The top angle beta will be as large as possible to achieve the highest ratio between the actuation force and contact forces. The proximal and middle connection segments will be S-shaped. Although the results of the C-shaped segment indicated better results, the C-shaped segment increases buckling phenomena in the actuation segment. In addition, high local stresses are expected due to large rotations in the connection point between the actuation segment and the connection segment, as in the straight connection segment. In order to achieve a more uniform distribution of the contact forces, the lengths of the proximal, middle and distal phalange will be 30 mm, 20 mm and 15 mm respectively accordingly to the criteria.In figure 11 a PRB model and schematic representation of the compliant form of the topology for the conceptual design are presented.

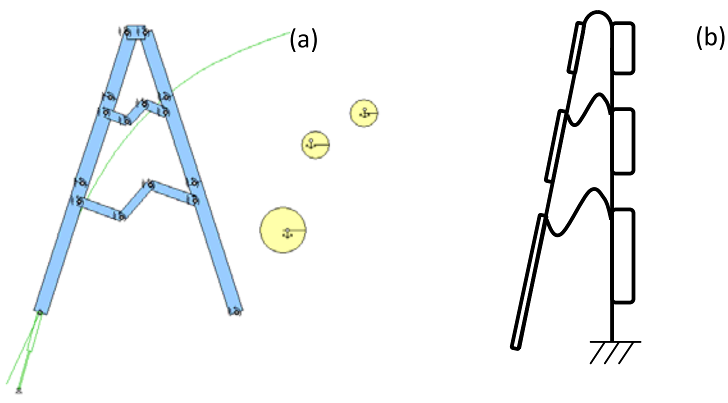

Figure 11: Topology of conceptual design, a) PRB model, b) Schematic representation of compliant model

Appendix [B]

Dimensional Analysis

The most promising topology of the finger (conceptual design) determined during the topology synthesis will be dimensioned in this section. The lengths and rotations will be determined based on the criterion and topology while the thickness of the various segments will be determined with non-linear PRB models.

Lengths and rotations

In figure 1 a schematic representation of the conceptual design in its compliant form is given with the various segments indicated.

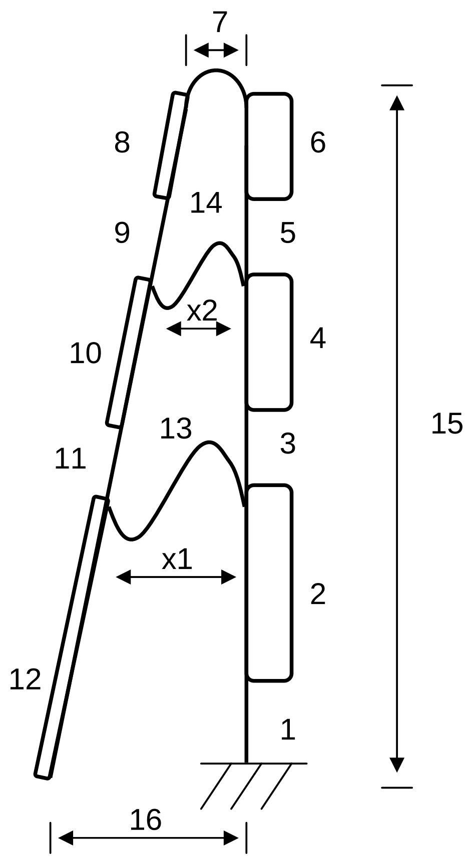

Parameter list:

- 1= L1, T1, $\alpha 1$
- 2= L2, T2
- 3= L3, T3, $\alpha 3$
- 4= L4, T4
- 5= L5, T5, $\alpha 5$
- 6= L6, T6
- 7= L7, T7, $\alpha 7$
- 8= L8, T8
- 9= L9, T9, $\alpha 9$
- 10= L10, T10
- 11= L11, T11, $\alpha 11$
- 12= L12, T12
- 13= L13, T13, $\alpha 13$
- 14= L14, T14, $\alpha 14$
- 15= L15, T15
- 16= L16, T16

Figure 1: Schematic representation of topology with various segments indicated

Criteria set 1, design space:
Length finger = 100 mm
Width finger = 30 mm
Thickness finger = 10 mm
Rotation joints = 30 degrees

This first criteria set leads to the dimensions of the following segments:

Table 1: Dimensions based on first criteria set

Parameter	Value
L15 (mm)	100
L16 (mm)	30
Alpha 1,3 and 5 (degrees)	30

Criteria set 2, anthropomorphic design:
Length joints, as small as possible
Ratio lengths fingers: Proximal finger 1, middle finger 2/3 and distal finger 1/2
Width top finger = 10 mm

A combination between the first criteria and second criteria sets lead to the dimensions of the following segments:

Table 2: Dimensions based on second criteria set

Parameter	Value
L1, L3, L5 (mm)	10
L2 (mm)	30
L4 (mm)	20
L6 (mm)	15
L7 (mm)	10

The final set of segments can be determined by utilizing the criteria, previously determined dimensions and the topology of the finger. The rotations of the segments are determined by executing a simulation with the Working Model program using a PRB model based on the determined dimensions.

Table 3: Dimensions based on second criteria set and topology of the finger

Parameter	Value
L8 (mm)	20
L9 (mm)	15
L10 (mm)	20
L11 (mm)	20
L12 (mm)	20
L13 (mm)	45
L14 (mm)	25
Alpha 7 max (degrees)	15
Alpha 9 max (degrees)	30
Alpha 11 max (degrees)	30
Alpha 13 max (degrees)	40
Alpha 14 max (degrees)	30

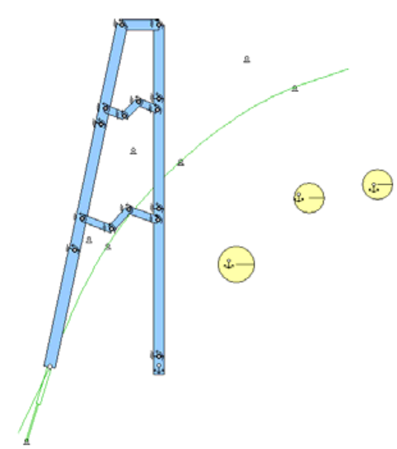

Figure 2: PRB model used to determine the rotations

Lengths L 13 and L 14 where determined based on the distances x1 and x2 and the height of the arc. The maximum rotation of the angles alpha 9,11,13 and 14 where approximated based on the geometric relations between the segments when the finger is in its maximal deviated orientation. These values where controlled by the simulation executed with the Working Model program.

Thickness compliant segments

The conceptual design has two types of segments, stiff non-deformable segments and flexible deformable segments. Segments 2,4,6,8,10 and 12 are stiff segments and segments 1,2,3,5,7,9,11,13 and 14 are flexible segments. The thickness of the stiff segments are determined merely based on the fact that they may not deform. The thickness of the flexible segments will be determined with Pseudo Rigid Body methods.

Stiff segments
The phalanges (2, 4 and 6) come in contact with the grasped object and may not deform at all. They should therefore be the stiffest parts of the design. The stiff parts in the actuation beam may be less stiff than the phalanges. The main function of these parts is to increase the overall stiffness of the actuation beam and prevent buckling. The thickness of the stiff segments were set at:

Table 4: Thickness of stiff segments

Parameter	Value
T2 (mm)	3
T4 (mm)	3
T6 (mm)	3
T8 (mm)	1
T10 (mm)	1
T12 (mm)	1

Flexible segments
The Pseudo Rigid Body method is used to determine the thickness of the flexible segments. Due to the large deformations in these segments (minimum deflection of 30 degrees), methods that account for non-linearity's must be used. Due to the difference in shape and the type of forces acting on the flexible segments, two different PRB methods are used:

- Straight beam theory with end moment for parts 1,3, 5, 9 and 11
- Initially curved beam theory for parts 13 and 14

In the following section the different theories and used formulas are described.

Models

All the used formulae and figures are taken from the book: Compliant elements by L.L. Howell [9].

Straight beam with Moment end:

In this case, a moment that acts on the end of the beam to deform the elastic segment. In figure 3 a schematic representation of the beam before and after deformation is presented.

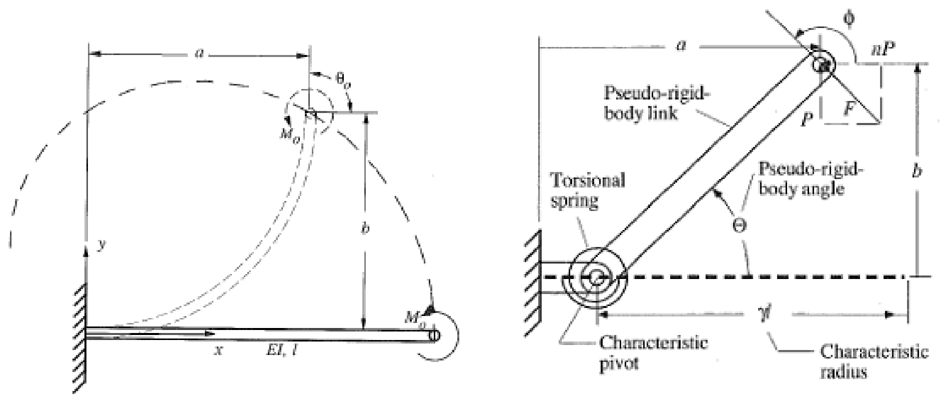

Figure 3: Compliant segment with moment at end and the PRB model of a compliant segment with variables indicated (Taken from Compliant elements by L.L Howell)

The elastic segment deforms over the entire length (l) of its body. The PRB model however has a link that remains fixed and a Pseudo Rigid Body link that can deviate. The length of this PRB link is $\gamma \cdot l$ with γ being the characteristic radius factor:

$$\gamma = 0.7346 \quad \text{constant value for end moment case} \qquad [1]$$

The deformation angle at the beams end of the elastic segment is represented by θ_0 .Because there is a nearly linear relationship between this angle and the Pseudo Rigid Body angle (Θ), a constant parametric angle coefficient (c_θ) can be identified that describes this relationship:

$$\theta_0 = c_\theta \cdot \Theta \quad \rightarrow \quad \Theta = \frac{\theta_0}{c_\theta} \text{ with } c_\theta = 1.5164 \quad \text{constant value for end moment case} \quad [3]$$

The elastic properties (stiffness) of the elastic segments are represented by a torsion spring in the PRB model. In order to determine the stiffness of this spring the stiffness coefficient (K_Θ) is used:

$$K_\theta = 2.0643 \quad \text{constant value for end moment case} \qquad [4]$$

The deflections of the beam end are:

$$\begin{aligned} a &= \left(1-\gamma\left(1-\cos(\Theta)\right)\right)\cdot l \\ b &= \left(\gamma \cdot \sin(\Theta)\right)\cdot l \end{aligned} \qquad [5,6]$$

The spring stiffness equals:

$$K = \gamma \cdot K_\theta \cdot \frac{E \cdot I}{l} \text{ or in this special case with end moment only } K = c_\theta \cdot \frac{E \cdot I}{l} \quad \text{with} \quad I = \frac{w \cdot h^3}{12}$$

The applied torsion/moment is:

$$M = K \cdot \Theta \qquad [8]$$

The maximal stress in the beam will equal:

$$\sigma = \frac{M \cdot c}{I} \quad \text{with} \quad c = \frac{h}{2} \qquad [9]$$

Initially curved beams:

For elastic segments that are non-straight, initially curved beam theory can be used. In this case, a force that acts on the end of the beam to deform the initially curved elastic segment. In figure 4 a schematic representation of an initially curved beam, before and after deformation is presented.

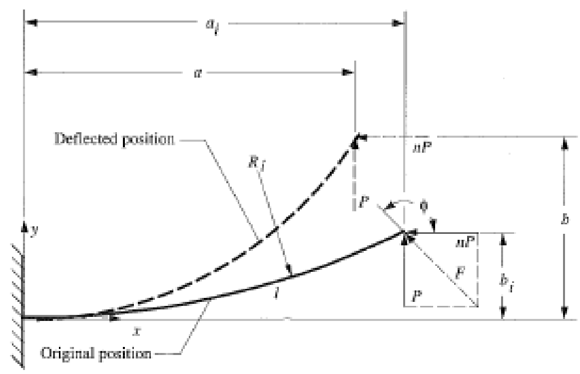

Figure 4: Compliant initially curved beam, before and after deflection (Taken from Compliant Elements by L.L. Howell)

At first the orientation of the actuation force (F), in respect to the horizontal, has to be defined. This is done by actuation angle (ϕ). The ratio between the vertical component (P) and horizontal component (Pn), of the actuation force, is determined by the factor n. This factor can be expressed in relation to the actuation angle as follow:

$$\phi = \tan^{-1}\left(\frac{1}{-n}\right) \qquad [10]$$

In this case where an initially curved beam will be deflected, the initial curve and coordinates of the end point of the beam need to be identified. A radius R_i and the non-dimensionalized parameter k_θ indicate the curve of the beam**:**

$$k_\theta = \frac{l}{R_i} \quad [11]$$

The initial coordinates of the end of the beam are:

$$a_i = \left(\frac{1}{k_\theta} \cdot \sin\left(k_\theta\right) \right) \cdot l$$
$$b_i = \left(\frac{1}{k_\theta} \cdot \left(1 - \cos\left(k_\theta\right)\right) \right) \cdot l \quad [12, 13]$$

With the initial coordinates of the end of the beam known the initial PRB angle $\left(\Theta_i\right)$ of the beam can be determined:

$$\Theta_i = \tan^{-1}\left(\frac{b_i}{a_i - l \cdot \left(1 - \gamma\right)} \right) \quad [14]$$

For initially straight beams, the radius factor γ was used to determine the length of the rigid body link. In case of an initially curved beam the length of the rigid body link is $\rho \cdot l$, where ρ, is a function of γ and the curvature and can be determined as follow:

$$\rho = \left\{ \left[\frac{a_i}{l} - \left(1 - \gamma\right) \right]^2 + \left(\frac{b_i}{l} \right)^2 \right\}^{1/2} \quad [15]$$

Besides calculating the parameter values γ, ρ and K_θ, the following table can be used in which recommended values for γ, ρ and K_θ for a certain k_θ are listed.

Table 5: Recommended values for the parameters γ, ρ and K_θ

k_θ	γ	ρ	K_θ
0.00	0.85	0.850	2.65
0.10	0.84	0.840	2.64
0.25	0.83	0.829	2.56
0.5	0.81	0.807	2.52
1.00	0.81	0.797	2.60
1.50	0.80	0.775	2.80
2.00	0.79	0.749	2.99

When the initial coordinates and PRB angle of the curved beam are known, the beams end coordinates after deflection can be determined:

$$a = \left(1 - \gamma + \rho \cdot \cos\left(\Theta\right)\right) \cdot l$$
$$b = \left(\rho \cdot \sin\left(\Theta\right)\right) \cdot l \quad [16, 17]$$

The stiffness will then be:

$$K = \rho \cdot K_{\Theta} \cdot \left(\frac{E \cdot I}{l} \right) \qquad [18]$$

The torsion at the hinge equals:

$$T = K \cdot \left(\Theta - \Theta_i \right) \qquad [19]$$

Combining equations to determine the applied force tangential to the PRB link path and the torsion will lead to the applied actuation force F_{total}:

$$\begin{array}{l} F_t = F \cdot \sin\left(\phi - \Theta\right) \\ T = \rho \cdot l \cdot F_t \end{array} \quad \rightarrow \quad F_{total} = \frac{T}{\rho \cdot l \cdot \sin\left(\phi - \Theta\right)} \qquad [20]$$

The applied vertical force P is:

$$P = \frac{F_{total}}{\eta} \quad \text{with} \quad \eta = \sqrt{1 + n^2} \qquad [21]$$

The maximum stress in the beam will then be:

$$\sigma = \frac{P \cdot \left(a + n \cdot b \right) \cdot c}{I} \quad \text{with} \quad c = \frac{h}{2} \qquad [22]$$

Input values:

To determine the thickness of the flexible segments the following parameters were used as fixed input values (depending on the type of flexible segment):

Table 6: Input values used to determine the thickness

Width (w, mm)	**Length (l, mm)**	**Deviation angle (θ, degrees)**	**Actuation force angle (ϕ, degrees)**
10	x	x	x

Parameters that were varied are the beam thickness and the type of material used:

Beam thicknes (h):
$x_1 < h < x_2$ mm, with steps $\Delta h = x_3$ mm

Materials investigated:

Table 7: Material properties of the various materials

Material type	*Youngs modulus (Pa)*	*Yield strength (Pa)*
1 Titanium (Ti6Al4V)	113.8e3	827
2 Steel (AISI630)	189.6e3	1276
3 Aluminium	71.7e3	324
4 Nithinol	80e3	900
5 Plastic	1.4e3	28

For each thickness a certain amount of stress will occur in the deformed elastic segment. Comparing this stress value with the maximum yield strength of the material will indicate the maximum allowable thickness of the elastic segment. In order to decrease the chance of fatigue and increase the amount of deformation cycles a safety factor of 1.25 is used for the maximum allowable stress in the material

$$\sigma_{safety} = \frac{\sigma_{\max}}{N_{factor}} \qquad [23]$$

The results will be presented in a table indicating the maximum allowable thickness for each type of material.

Results Joints

Using the earlier determined lengths, width, and deviation angle, the maximum thickness for the joints (segments 1, 3 and 5) are determined.

Theory:
Straight beam with end moment

Fixed parameters:

Table 8: Input values for segments 1, 3 and 5

Width (w, mm)	Length (l, mm)	Deviation angle (θ, degrees)
10	10	30

Variable values:
Beam thickness (h)
$0.01 < h < 1\ mm$, with steps $\Delta h = .01\ mm$

Results:

Table 9: Results segments 1, 3 and 5

Material type	Type 1	Type 2	Type 3	Type 4	Type 5
Max thickness (mm)	0.22	0.20	0.13	0.34	0.61

Results actuation segments

- Thickness for the bottom actuation segment (segment 11)

Theory:
Straight beam with end moment

Fixed parameters:

Table 10: Input values segment 11

Width (w, mm)	Length (l, mm)	Deviation angle (θ, degrees)
10	20	30

Variable values
Beam thickness (h)
$0.1 < h < 2\ mm$, with steps $\Delta h = .01\ mm$

Results:

Table 11: Results of segment 11

Material type	Type 1	Type 2	Type 3	Type 4	Type 5
Max thickness (mm)	0.44	0.41	0.27	0.68	1.22

- Thickness for top actuation segment (segment 9)

Theory:
Straight beam with end moment

Fixed parameters:

Table 12: Input values segment 9

Width (w, mm)	**Length (l, mm)**	**Deviation angle (θ, degrees)**
10	15	30

Variable values
Beam thickness (h)
$0.1 < h < 1\ mm$, with steps $\Delta h = .01\ mm$

Results:

Table 13: Results of segment 9

Material type	Type 1	Type 2	Type 3	Type 4	Type 5
Max thickness (mm)	0.33	0.30	0.20	0.51	0.91

Connection segments

For the initially curved beam the curve of the segment has to be defined. Due to the fact that only simple curved beams with a certain radius (Ri) can be modelled with this theory, segments 13 and 14 were modelled as two connected C-shaped beams (fig 5a-c). The rotations of the C-shape at the actuation segment side are smaller than the rotations of the C-shape on the phalanx side. This results in the use of two separate models. Assuming that each C-shaped segment has symmetrical properties, the C-shapes can be modelled as two curved segments each taking account for half the total deflection. In order to achieve a connection segment with a uniform thickness the lengths of the two modelled C-shapes will differ. Segment 7 consists out of a single C-shape and therefore will be modelled as two symmetrical initially curved segments.

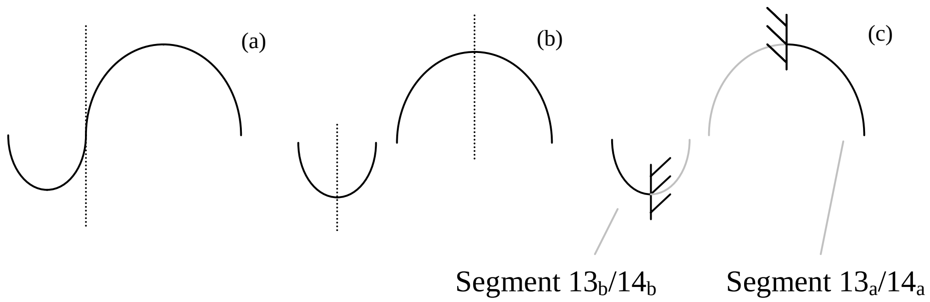

Figure 5 a-c: Models of the connection segments, (a) Single segment (b) Two C-shaped segments (c) Four initially curved segments

Thickness for the bottom connection segment (segment 13), first the curved beams on the phalanx side (13_a) are modelled second the curved beams on the actuation side (13_b).

- Segment 13_a

Fixed parameters:

Table 14: Input values segment 13_a

Width (w, mm)	**Length (l, mm)**	**Deviation angle (θ, degrees)**	**Actuation force angle (ϕ, degrees)**	**Parameter k_θ**
10	15	35	90	1.65

Variable values
Beam thickness (h)
$0.01 < h < .5\ mm$, with steps $\Delta h = .01\ mm$

Results:

Table 15: Results of segment 13_a

Material type	Type 1	Type 2	Type 3	Type 4	Type 5
Max thickness (mm)	0.12	0.11	0.07	0.19	0.34

- Segment 13_b

Fixed parameters:

Table 16: Input values segment 13_b

Width (w, mm)	**Length (l, mm)**	**Deviation angle (θ, degrees)**	**Actuation force angle (ϕ, degrees)**	**Parameter k_θ**
10	7.5	25	90	1.5

Variable values
Beam thickness (h)
$0.01 < h < .5\ mm$, with steps $\Delta h = .01\ mm$

Results:

Table 17: Results of segment 13_b

Material type	Type 1	Type 2	Type 3	Type 4	Type 5
Max thickness (mm)	0.14	0.13	0.09	0.22	0.40

Thickness for the top connection segment (segment 14), first the curved beams on the phalanx side (14_a) are modelled second the curved beams on the actuation side (14_b).

- Segment 14_a

Fixed parameters:

Table 18: Input values of segment 14_a

Width (w, mm)	**Length (l, mm)**	**Deviation angle (θ, degrees)**	**Actuation force angle (ϕ, degrees)**	**Parameter k_θ**
10	7.5	25	90	1.5

Variable values
Beam thickness (h)
$0.01 < h < .5\ mm$, with steps $\Delta h = .01\ mm$

Results:

Table 19: Results of segment 14_a

Material type	Type 1	Type 2	Type 3	Type 4	Type 5
Max thickness (mm)	0.14	0.13	0.09	0.22	0.40

- Segment 14_b

Fixed parameters:

Table 20: Input values of segment 14_b

Width (w, mm)	Length (l, mm)	Deviation angle (θ, degrees)	Actuation force angle (ϕ, degrees)	Parameter k_θ
10	5	15	90	1.5

Variable values
Beam thickness (h)
$0.01 < h < 1\ mm$, with steps $\Delta h = .01\ mm$

Results:

Table 21: Results of segment 14_b

Material type	Type 1	Type 2	Type 3	Type 4	Type 5
Max thickness (mm)	0.58	0.53	0.36	0.90	1

- Segment 7

Fixed parameters:

Table 22: Input values of segment 14_b

Width (w, mm)	Length (l, mm)	Deviation angle (θ, degrees)	Actuation force angle (ϕ, degrees)	Parameter k_θ
10	5	15	90	1.5

Variable values
Beam thickness (h)
$0.01 < h < 1\ mm$, with steps $\Delta h = .01\ mm$

Results:

Table 23: Results of segment 14_b

Material type	Type 1	Type 2	Type 3	Type 4	Type 5
Max thickness (mm)	0.58	0.53	0.36	0.90	1

Final results dimension analysis:

The final dimensions of the conceptual design that will be used as input for the finite segment analysis are presented in table 24. In order to achieve a flexible segment with a uniform thickness, the thicknesses of segments 13_a and 14_a will be used for the entire segments 13 and 14. The material used for the conceptual design will consist out of titanium (appendix E).

Table 24: Overview of the dimensions of the conceptual design

Segment	**1**	**2**	**3**	**4**	**5**	**6**	**7**	**8**	**9**	**10**	**11**	**12**	**13_a**	**13_b**	**14_a**	**14_b**
Length (mm)	10	30	10	20	10	15	10	20	15	20	20	20	15	7.5	7.5	5
Thickness (mm)	0.22	3	0.22	3	0.22	3	0.58	1	0.33	1	0.44	1	0.12	0.14	0.14	0.58
Rotation (degrees)	30	-	30	-	30	-	15	-	30	-	30	-	35	25	25	15

Mock-ups

Four mock-ups were created to control and verify the kinematics of the conceptual design. Two plastic and two stainless steel models were created.

During tests with the mock-ups an additional criteria was introduced. Initially a curved actuation path was used, however due to the lack of space inside a prosthetic device and the difficulty of integrating such a path in the design it was chosen to actuate the finger along a vertical path. This criterion along with the execution of a type synthesis and dimensional analysis resulted in the elongation of segment 12 and the addition of a flexible segment (segment 15) in the conceptual design. The topology of the stainless steel mock-ups existed out of this new conceptual design and verified the kinematical requirements.

The final dimensions of the conceptual design are presented in table 25, the PRB model used for the type synthesis and dimensional analysis of the final conceptual design is presented in figure 6.

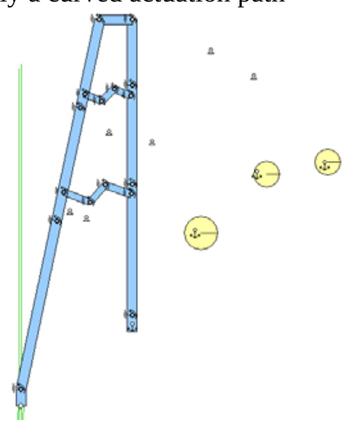

Figure 6: PRB model of the conceptual design with vertical actuation

Table 25: Overview of the dimensions of the final conceptual design

Segment	**1**	**2**	**3**	**4**	**5**	**6**	**7**	**8**	**9**	**10**	**11**	**12**	**13**	**14**	**15**
Length (mm)	10	30	10	20	10	15	10	20	15	20	20	40	45	25	15
Thickness (mm)	0.22	3	0.22	3	0.22	3	0.58	1	0.33	1	0.44	1	0.12	0.14	0.24
Rotation (degrees)	30	-	30	-	30	-	15	-	30	-	30	-	40	30	40
Width (mm)	10	10	10	10	10	10	10	10	10	10	10	10	10	10	10

Appendix [C]

Buckling

Buckling indicates the failure mode of a beam that is subjected to compressive stresses. The point when the applied compressive stresses are higher than the ultimate compressive stresses that the material can withstand, the buckling point has been reached. The buckling point can be determined as follow:

$$F = \frac{\pi^2 \cdot E \cdot I}{(K \cdot l)^2}$$

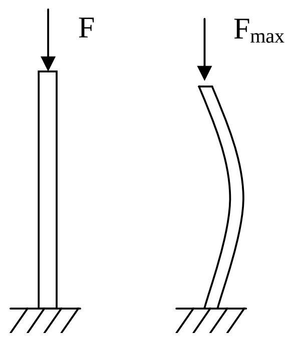

Figure 1: Buckling of a beam with a fixed and a free end

In these formulas K represents the effective length of the beam, which is a fixed value and depends on the type of connection between the beam and the surface. In these cases there is one fixed end and one free end moving latterly resulting in a value of 2 for K.

Table 1: Maximal axial force until buckling phenomena are initiated

Element	**1**	**3**	**5**	**9**	**11**	**15**
Thickness (mm)	0.21	0.19	0.18	0.26	0.37	0.25
Length (mm)	13	13	13	21	27	15
Max Force (N)	12.8	9.5	8.1	9.3	16.3	16.2

Torsion

Besides bending the flexible elements can also be subjected to torsion. In order to determine whether the flexible elements of the conceptual design can withstand torsion, their maximal torsion stiffness is determined. Formulas used are:

$$T = \tau_{\max} \cdot \alpha \cdot b \cdot h^2$$

In this equation α represents a constant value that can be determined from a table were several ratios between h and b $\left(\frac{b}{h}\right)$ are related to a value of α.
In this case α =1/3

When the amount of Torsion acting on the beam is known, the amount of rotation due to the Torsion can be determined:

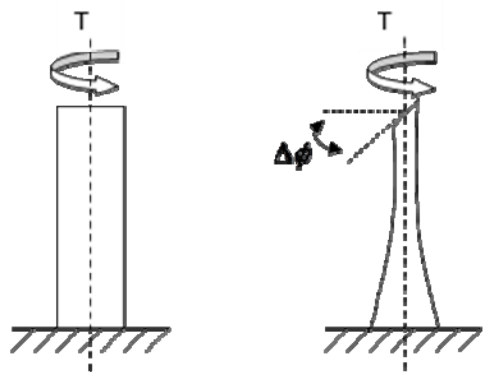

Figure 2: Torsion and rotation of beam

$$\Delta\phi = \frac{T \cdot l}{\beta \cdot b \cdot h^3 \cdot G}$$

In this equation β represents a constant value that can be determined from a table were several ratios between h and b $\left(\frac{b}{h}\right)$ are related to a value of β. In this case β =1/3

Fem Analysis
The initial simulations of the FEM analysis indicated that the allowable stress in the elements was exceeded. In order to reduce the stress the elements need to become more flexible by either elongating or reducing the thickness of the element. Increasing the flexibility of the element also induces negative aspects such as rotation around the axes of the element. The influence of increasing the length or reducing the thickness on the Torsion stiffness of the element is investigated.

Two simulations were executed. One with a fixed length (l = 10) and variable thickness (h=0.15:0.01:0.21) and one with a variable length (l = 10:1:15) and fixed thickness (h=0.21). The results indicate that decreasing the thickness of the elements has a larger negative influence on the torsion stiffness of the elements. Reducing the stress in the elements will therefore initially be achieved by elongating the elements.

Table 2: Maximal allowable torque and the resulting rotation of the segments

Element	**1**	**3**	**5**	**15**
Thickness (mm)	0.21	0.19	0.18	0.25
Length (mm)	13	13	13	15
Max Torque (N-mm)	465	420	398	553
Max Rotation (degrees)	273	334	372	222

Appendix [D]

Finite Element Analysis

In order to execute the numerical analysis it was chosen to use Finite Element analysis methods (FEM) due to the authors experience with this method and the availability of an FEM simulation program (Ansys V11).

The conceptual design was used as input for the FEM analysis. The conceptual design was modeled by defining key points and lines connecting them in order to define the outline of the model (fig 1). Areas were created between the lines and meshed to obtain elements required for the FEM analysis. Plane 42 Solid elements were used and a fine meshing process was utilized to increase the number of elements and therefore the accuracy of the model. Using Solid elements does increase the computation time of the simulation in respect to simple Beam elements. However, due to the fact that elements with different and in a later phase non-uniform thickness were modeled, using BEAM elements resulted in high stresses in the connection points and the inability to model the elements.

A set of parameters was used to define the thickness of the various elements, the actuation displacement, actuation force and some fixed key points. Variable key points were defined as a function of the thickness. In this way different designs could be obtained by merely changing the parameters (thickness of the elements) in the code of the batch file.

In order to reduce the computation time and increase the chance of the simulation converging to a solution, a large amount of constraints must be used. In this case all the lines defining the base block were fixed to their position and the actuation block was reduced to movements only in the y-direction (fig 3). Using a displacement instead of a force as actuation also increases the chance of the simulation converging to an answer.

Due to large deflections of the elements, non-linear analysis must be used for the simulations. This was achieved by applying LARGE DISPLACEMENT STATIC analysis type in the FEM analysis. Defining a large number of sub-steps will result in obtaining an accurate force-displacement curve of the actuation point and reaction forces.

Three linear springs were used to obtain the maximal deflected orientation of the finger and determine the reaction forces in order to achieve this orientation. COMBIN 14 elements in which the stiffness of the spring (k) is used were used to model the springs. The springs were modeled by simply defining a line as a COMBIN 14 element, constraint at one end in all directions and attached to a node in the phalanx on the other end. The meshing procedure for this element must be done manually in order to obtain a single spring element ($k_{spring} = k_{input}$). Otherwise the program will divide the line in multiple elements resulting in multiple springs connected to each other in series ($k_{spring} = \frac{k_{input}}{n_{elements}}$).

During each simulation a displacement was applied at the actuation block resulting in the maximal deflected orientation of the finger. The orientation and rotation of the phalanges was determined by evaluating the coordinates of the key-points defining the phalanges. Subsequently the reaction forces in the fixed connection points of the springs defined the required contact forces acting on the phalanges.

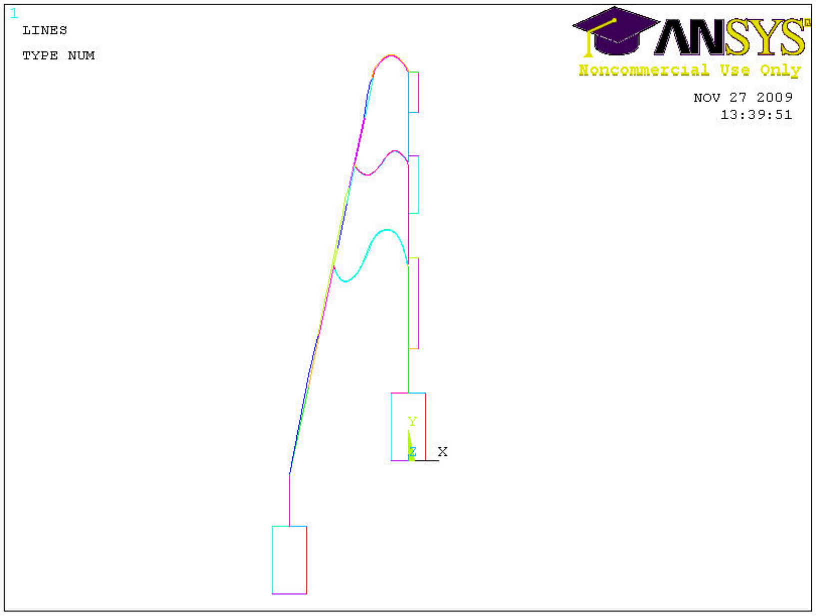

Figure 1: Outline of the finger model in the ANSYS V11 simulation environment

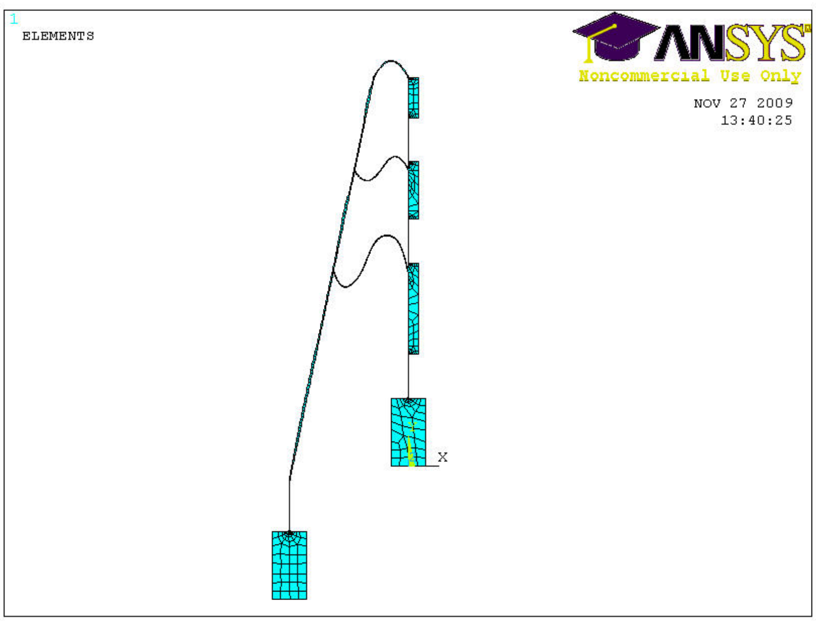

Figure 2: Meshed area of the finger model in the ANSYS V11 simulation environment

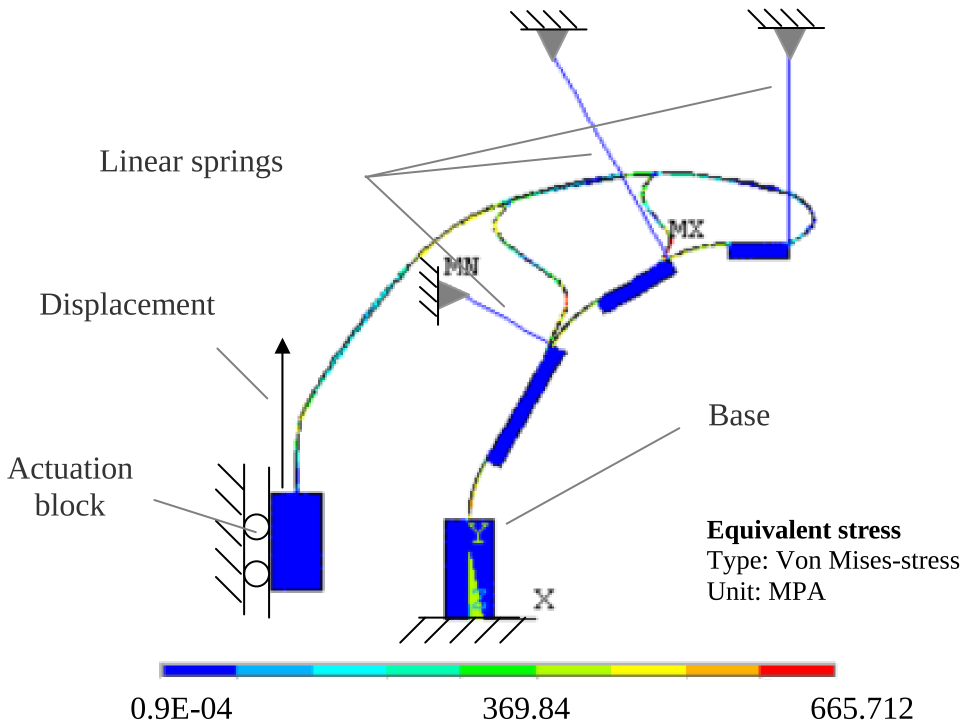

Figure 3: Von Mises-stress of the titanium finger in the maximal deflected orientation in the ANSYS simulation environment

Appendix [E]

Material and Fabrication:

The type of material used for the conceptual design influences the dimensions of the design significantly. Aspects as manufacturing capabilities, durability, cost and reliable material properties are taken into account when choosing the type of material.

Two different types of materials were considered:

- Metals
- Plastics

Comparing the advantages and disadvantages of both materials indicated that the use of metals is the better option for the final design. Increase of durability and robustness, good manufacturing capabilities, predictable material properties and lower susceptibility to creep where the main reasons for using a metallic material.

Within the metal group four different types where considered:

- Stainless steel (AISI 360)
- Titanium (Ti-6Al-4V)
- Aluminium
- Nitinol

A comparison between the several options revealed that two types of materials most likely to be used are: Stainless steel and titanium. Aluminium has the lowest yield strength to Young's modulus ratio and although nitinol has the best elastic properties (super-elastic material) it is very expensive and has little manufacturing capabilities.

Possible manufacturing methods are EDM machining and laser-cutting. A big influence on the accuracy of these manufacturing methods is the thickness of the material. Within laser-cutting the maximal thickness to acquire a good accuracy is 1 mm. The final design can then only be acquired by adding several layers together. This is not beneficial for the design and working characteristics of the design. The maximal thickness of the material with EDM machining is 5 mm. In this case the design can be obtained directly with a high accuracy.

Experience of fabricators indicated that titanium for thin-walled constructions, such as the design, would result in a higher accuracy during fabrication and in the lowest possibility of the walls fracturing during fabrication. Due to these reasons and the fact that titanium has a higher strength to Young's modulus ratio then stainless steel, titanium will be used as material for the final design.